Crustal Earthquake Instability in Relation to the Depth Variation of Frictional Slip Properties

Simon T. Tse[1]

Division of Applied Sciences, Harvard University, Cambridge, Massachusetts

James R. Rice

*Division of Applied Sciences and Department of Earth and Planetary Sciences
Harvard University, Cambridge, Massachusetts*

Recent stability studies using constitutive relations of the type found by Dieterich, Ruina, and others to describe frictional slip of rocks in the laboratory have provided a new explanation of the depth cutoff of shallow crustal earthquakes. The class of friction laws discussed has the property that the sliding stress depends on normal stress, temperature, slip rate, and slip history. For sliding at a fixed slip rate V and fixed environment (e.g., normal stress, temperature, etc.) the shear strength τ evolves toward a steady state value $\tau^{ss}(V)$. Stability analysis show that for $d\tau^{ss}(V)/dV < 0$ (i.e., velocity weakening), steady state sliding is unstable to any perturbation in systems of sufficiently low stiffness and is unstable to sufficiently large perturbations in systems of higher stiffness. Hence a surface with $d\tau^{ss}(V)/dV < 0$ is potentially unstable. Conversely, $d\tau^{ss}(V)/dV > 0$ (velocity strengthening) implies stable steady state sliding, at least for a broad class of constitutive laws more fully described in the paper. Experiments by Dieterich and by Tullis and Weeks on Westerly granite with mature sliding surfaces indicate that $d\tau^{ss}(V)/dV$ is negative at room temperature, whereas higher-temperature experiments by Stesky show that $d\tau^{ss}(V)/dV$ becomes positive above approximately 300°C. Therefore, in the case of the earth, where temperature increases with depth, the above observations seem to suggest that the depth cutoff of crustal earthquake activity can be understood in terms of the variation of the frictional response with depth, from a regime with $d\tau^{ss}(V)/dV < 0$ to one with $d\tau^{ss}(V)/dV > 0$. This is not inconsistent with, but rather refines, the suggestion by Sibson and others that the depth cutoff is due to a transition from brittle friction to ductile flow. Further, our results show definitively that the shallow depth confinement of seismicity is compatible with a model in which deformation is localized to a fault zone extending well below the seismogenic depth. The depth confinement does not require a model showing transition to a zone of broadly distributed creep flow beneath the seismogenic zone. Following Mavko, a two-dimensional quasi-static strike-slip fault model is analyzed but using different numerical procedures and a depth variation of frictional properties based on the laboratory data mentioned above and the Lachenbruch-Sass depth variation of temperature for the San Andreas fault. The resulting predictions of such features as the confinement of crustal earthquakes to shallow depths, the development of locked patches, the recurrence time for the seismic cycle, the seismic stress drop and displacement, etc., are generally in agreement with the observed characteristics of large-scale strike-slip earthquakes along the San Andreas fault. Calculations based on the laboratory data predict, for example, that stick slip nucleates around 5–7 km, that large seismic motion occurs around the nucleation depth and above but diminishes gradually to zero at 13–15 km depths, that rapid postseismic creep occurs over another 3–4 km depth, and that at greater depths, steady slip consistent with the average plate velocity is only modestly perturbed by the earthquakes occurring above. The most uncertain parameter is the slip weakening distance L for evolution of fault surface state; we illustrate how features of the predicted earthquake cycles vary with L over the range for which calculations are feasible.

INTRODUCTION

It has been observed that crustal earthquakes, which are generally thought to arise from unstable frictional sliding on preexisting fault surfaces [*Brace and Byerlee*, 1966; *Dieterich*, 1974], occur predominately at shallow depths along transform margins [*Eaton et al.*, 1970; *Hill et al.*, 1975; *McHugh and Lester*, 1978; *Wesson et al.*, 1973; *Sibson*, 1982]. For example, along the San Andreas fault in central California, the vast majority of seismicity is confined to the upper 12 km of the crust. This shallow depth confinement of seismicity is commonly explained by the change of deformation mechanism from pressure-sensitive brittle frictional sliding at shallow depths to temperature-sensitive aseismic ductile flow at lower

depths [*Meissner and Strehlau*, 1982; *Sibson*, 1982, 1983; *Chen and Molnar*, 1983]. Stresses are relaxed considerably in the ductile flow regime from the levels that would be required for rapid (seismic) slip. Within this model as enunciated, e.g., by Sibson, the depth at which the deformation mechanism changes from brittle to ductile corresponds to the greatest seismogenic depth. Based on the assumption of the Byerlee friction law in the brittle zone and the power law creep flow of a quartzlike mineral below, *Sibson* [1982] explained in this way a limiting seismogenic depth along the San Andreas fault of about 10–15 km, at which the temperature is about 300°–350°C. This model is usually interpreted as implying a peak resistance and a sharp brittle-ductile transition at the base of the seismogenic layer, although the mechanics by which the earthquake instability comes about is not explicitly included in the model.

There seems to be a tacit assumption in this type of description that a zone which deforms by frictional sliding will necessarily do so in an unstable stick-slip mode, i.e., seismically.

However, there is evidence that the frictional sliding process itself may be either of a stable or unstable type. We show here that the transition from one mode of friction to the other is of itself sufficient to provide an explanation for the depth confinement of crustal seismicity. Also, our results imply that the observed depth confinement does not require for its explanation that the seismically active portion of plate boundary be underlain by a zone of broadly distributed creep flow, as is occasionally assumed in discussions of friction to creep transitions. The depth confinement is equally compatible with a model in which deformation at the plate boundary is confined to a narrow fault zone over a depth considerably greater than that of seismic activity before giving way to broadly distributed creep. The latter geometry is, in fact, closer to that suggested by *Sibson* [1977, 1982, 1983, 1984], who argues on geologic evidence for localized aseismic shearing below the seismogenic region in tabular mylonite zones of tens to hundred of meters thickness.

It is observed along the San Andreas fault system that some shallow fault zones creep aseismicially, while others, presumably of somewhat different mineralogy but having comparable temperature and normal stress, deform seismically. Also, laboratory experiments on rocks of the type initiated by *Brace and Byerlee* [1966] show that the stability of frictional sliding depends on environmental conditions such as pore pressure, rock type, porosity, gouge layer thickness and size, and more importantly on temperature and effective normal pressure. Low temperature and high pressure tend to destabilize sliding. These early experiments were carried out in a manner which did not lead to a full mechanical basis for analyzing the stability of frictional sliding. However, that situation has been improved upon through friction experiments on Westerly granite and quartzite by *Dieterich* [1978, 1979a, b, 1980, 1981], *Ruina* [1980, 1983], *Tullis and Weeks* [1986], and others. The experiments have resulted in a class of constitutive relations for frictional slip resistance which depend on slip rate and slip history as well as on the other environmental factors mentioned above; see *Ruina* [1983] for a summary of such constitutive relations. For sliding at fixed environments and fixed speed, the frictional stress τ between sliding surfaces is found to evolve with ongoing slip towards a steady state value $\tau^{ss}(V)$. The experiments mentioned above together with the high-temperature experiments done by *Stesky* [1975, 1978] on Westerly granite and gabbro indicate that the quantity $d\tau^{ss}(V)/dV$ (long-term rate sensitivity) changes from negative (velocity weakening) at low temperatures to positive (velocity strengthening) at high temperatures.

The significance of this transition can be judged from stability analyses by *Ruina* [1980, 1983], *Rice and Ruina* [1983], *Gu et al.* [1984], and *Rice and Gu* [1983]. They show that if $d\tau^{ss}/dV < 0$, steady state sliding is unstable in systems of sufficiently low stiffness or in stiff systems subjected to sufficiently strong perturbations from steady state. Otherwise, sliding is stable when $d\tau^{ss}/dV > 0$. Specifically, these conclusions on the relevance of the sign of $d\tau^{ss}/dV$ to stability follow from two sources. One is the full nonlinear analysis of motion of a single degree of freedom spring and sliding block system following the specific frictional constitutive relation of equations (2)–(4) which follow and involving a single evolving state variable. The other source is the general linearized analysis of the stability of steady state slip to small perturbations for the broad class of constitutive laws which need show only positive instantaneous rate sensitivity and monotonic approach of stress

τ to $\tau^{ss}(V)$ in slip at constant speed V following a step change from the speed of a previous steady state. (Nevertheless, *Weeks and Tullis* [1984, 1985] present an exception to such monotonic approach for dolomite, and stability in that case may not be determined solely by $d\tau^{ss}/dV$.) Hence applying the experimental data and the consequence of the stability analysis to the crust, one can propose an explanation for the shallow depth of seismicity in terms of the change of nature of a frictional sliding property from velocity weakening at cool, shallow depths (possibly unstable sliding) to velocity strengthening (stable sliding) at hot, greater depths [*Tse and Rice*, 1984]. Most of the stability analysis referred to above was done for single degree of freedom spring block systems. *Mavko* [1980, also unpublished manuscript, 1984], without appealing to an experimental basis for the transition, showed for strike-slip sliding between elastic blocks that a transition in sign of $d\tau^{ss}/dV$ with depth does indeed confine instability to shallow depths.

Depending on the rheology, the depth estimated for transition from unstable to stable frictional slip on a deeply penetrating crustal fault may or may not be the same as the depth estimated for the transition from frictional sliding to general creep relaxation, based on quartz flow properties, by Sibson and others. In terms of deformation micromechanisms, it is possible that the transition with temperature from unstable to stable frictional sliding comes about from a thermal softening of the quartz constituent of granitic rocks. To the extent that it is this same thermal softening of quartz which allows the creep relaxation as envisioned by Sibson and others to take place (or at least would allow if conditions for creep of quartz correspond to those for general creep of a polymineralic mid to lower crust), one might expect that transition depths based on the two approaches will be more or less comparable. In fact, the form that we propose for our "frictional sliding" constitutive relations has the feature that at sufficiently high temperature (above approximately 400°C), the dependence on slip history disappears and the relations reduce to a nonlinear viscous creep relation between τ and slip rate. Further, τ at depth relaxes substantially below the value required for rapid slip, just as envisioned in the Sibson approach. Our constitutive relations, however, have also the advantage of fully predicting processes leading to instability as well as afterslip and the regain of strength of the fault surface at shallow depths as required to model sequences of tectonic earthquakes.

While the actual stressing and deformation process through the earth's crust and upper mantle is not fully documented, several crustal scale models have been proposed to simulate the stick-slip instability and its shallow depth confinement. One such model is the slip weakening model [*Stuart*, 1979a, b; *Stuart and Mavko*, 1979] in which the fault surface is prohibited from sliding if the frictional resistance is less than a critical value but begins to slide when the resistance becomes equal to the critical value. Once the slip commences, the resistance evolves toward a lower residual level gradually with ongoing slip. The slipping is unstable if the rate of decrease in resistance with slip is faster than the rate of elastic unloading of the surroundings, and otherwise it is stable. Hence the shallow depth confinement of the seismicity is achieved in such models by varying with depth the magnitude of the drop from the critical to residual strength level. Another model is the crack model [*Li and Rice*, 1983] in which an aseismic slip zone below the seismogenic depth is simulated by sliding of the crack planes under constant resistance while the locked sec-

tion in the seismogenic layer is represented by the uncracked fault plane. The critical fracture energy for advance of the slipping region into the locked region is taken to be depth variable. As discussed by Li and Rice, this cracklike model can be regarded as a limiting case of the slip weakening model if the size of the zone of strength degradation is much smaller than characteristic crustal dimensions. A shallow depth earthquake instability corresponds to unstable upward progression of the slip zone into the seismogenic layer. It is thought that a superior description of slip weakening, adequate to explain also such phenomena as strength regain in (nearly) stationary contact, is provided by the slip rate and slip history dependent laws of the class discussed in the previous paragraph. *Mavko* [1980, also unpublished manuscript, 1984] has used these to model earthquake instabilities in a strike-slip environment. By arbitrarily changing the friction property $d\tau^{ss}/dV$ from velocity weakening at shallow depths to velocity strengthening at greater depths, Mavko was able to simulate the shallow depth confinement of seismicity. Although the above models are able to produce the depth cutoff of seismicity, it should be noted that all do so by assuming rather arbitrary property variations with depth that do not have a direct experimental basis.

In our work here, we follow *Mavko* [1980, also unpublished manuscript, 1984] in applying the slip rate and slip history dependent constitutive relations in a strike-slip environment. However, to the limited extent that is presently possible, we attempt to constrain the depth variation of frictional constitutive properties based on laboratory temperature and normal stress dependence for granite and based on geotherms that are thought to be appropriate for the San Andreas fault. The result is an apparently realistic description of the depth confinement of faulting although there are very large gaps in the experimental data.

FRICTIONAL RESPONSE TO VARIABLE SLIP HISTORY

The class of the rate and slip history dependent friction law mentioned earlier has emerged from laboratory studies on rocks of the type initiated by *Dieterich* [1979a, b, 1980, 1981] and *Ruina* [1980, 1983, 1984] and carried on by a number of other researchers. Observations from these studies suggest that the instantaneous frictional response due to a sudden change in slip speed V is positive; i.e., $(\partial\tau/\partial V)_{inst} > 0$. Also, for slip motion at constant V and effective normal stress σ_n, it seems that τ evolves with ongoing slip toward a steady state value $\tau^{ss} = \tau^{ss}(V)$ dependent on that speed. We introduce the notations

$$A = V(\partial\tau/\partial V)_{inst} = (\partial\tau/\partial \ln V)_{inst}$$

$$A - B = V\, d\tau^{ss}/dV = d\tau^{ss}/d \ln V$$

Here for given σ_n and environment, A is to be regarded as a function of V and the previous slip history (or of the current "state" of the surface) in general; in the second relation, A is evaluated at steady state conditions, being then dependent on V only, and B is also a function of V in general. In fact, experimental data at low slip speeds characteristic of preinstability slip seems to be fit tolerably by regarding A and B as constant at fixed σ_n and environment, i.e., independent of V and the previous slip history. (It would be sensible to introduce a new symbol, say, C for what we call $A - B$ here but precedent which stems from an equation written as in equation (4) to follow dictates the introduction of B.)

A can be thought of as characterizing the instantaneous rate

sensitivity, while $A - B$ characterizes the long-term rate sensitivity. Hence depending on whether $A - B$ is positive or negative, the frictional response is either velocity strengthening or velocity weakening, respectively. The explicit dependence of A and B on σ_n is not fully known, but room temperature experiments at low σ_n (of order 10 MPa from Dieterich's and Ruina's experiments) and at high σ_n (up to 75 MPa in experiments by *Tullis and Weeks* [1986]), give values for A/σ_n and B/σ_n in the same range. As will be seen, data for A/σ_n at 300°C and $\sigma_n \simeq 500$ MPa also gives values comparable to the room temperature values. Such results suggest that A and B are approximately proportional to σ_n at low and possibly up to moderate temperatures. At higher temperatures for which temperature-sensitive ductile flow occurs in some or all constituents of the adjoining rock, it is plausible that A and B are less dependent on, or ultimately independent of, σ_n.

Dieterich's [1981] experiments on sliding of two intact Westerly granite blocks, with gouge layers of the same material between them but variable gouge particle size, layer thickness, and surface roughness of the adjoining rock are well described with A and B independent of V over his test range from 0.25 to 25 μm/s. Further, one finds $A/\sigma_n = 0.006$ to 0.008 for a rough surface (r) and 0.003 to 0.005 for a smooth surface (s), whereas $(A - B)/\sigma_n = -0.0007$ to -0.0011 for (r) and -0.002 to -0.006 for (s). In rotary shear experiments on Westerly granite, over the velocity range from 0.01 to 10 μm/s, with about 150-μm-thick gouge layer developed from initially bare rock surface and normal pressure up to 75 MPa, *Tullis and Weeks* [1986] found that $(A - B)/\sigma_n = -0.0015$ to -0.004 for total slip ranging from 10 mm to 70 mm. Experiments by *Solberg and Byerlee* [1984] and *Vaughan and Byerlee* [1985] on Westerly granite gouge in the sawcut triaxial apparatus show velocity strengthening (positive $A - B$), but it seems possible in view of their large scatter in reported rate sensitivity and general lack of reproducibility that these tests involved significant evolution of the gouge throughout their limited feasible displacement and did not achieve steady state conditions. The discrepancy with results already noted needs to be resolved in further experimentation. We have found results on high temperature (300°C–700°C) frictional slip in earlier work by *Stesky* [1975, 1978], done before the current approach to friction via constitutive relations was established. He reported results for sliding in prefaulted Westerly granite and gabbro triaxial specimens under 250 MPa confining pressure and found that at a given temperature both the instantaneous and long-term (steady state) variations in stress, after a sudden change in imposed deformation rate, were approximately linear in $\ln V$ over the entire range examined from 0.1 μm/s to 0.1 mm/s. Hence we can interpret his results as suggesting that A and B are approximately constant for given σ_n and temperature. His results, reported as variations of A/σ_n and $(A - B)/\sigma_n$ with temperature are summarized as the open symbols in Figure 1. The actual values of A and $A - B$ for his tests are also indicated. Note that $(A - B)/\sigma_n$ at room temperature is negative (velocity weakening) while at temperatures above 300°C, both $(A - B)/\sigma_n$ and A/σ_n are positive (velocity strengthening) and increase with temperature. This suggests that the frictional response becomes more viscous and ductile at higher temperature. Although there seems to be no experimental data which would help to constrain A and B in the temperature range from room temperature up to about 300°C, it is interesting to note that *Stesky* [1975, 1978] reported that his preliminary experiments below 250°C tended to exhibit
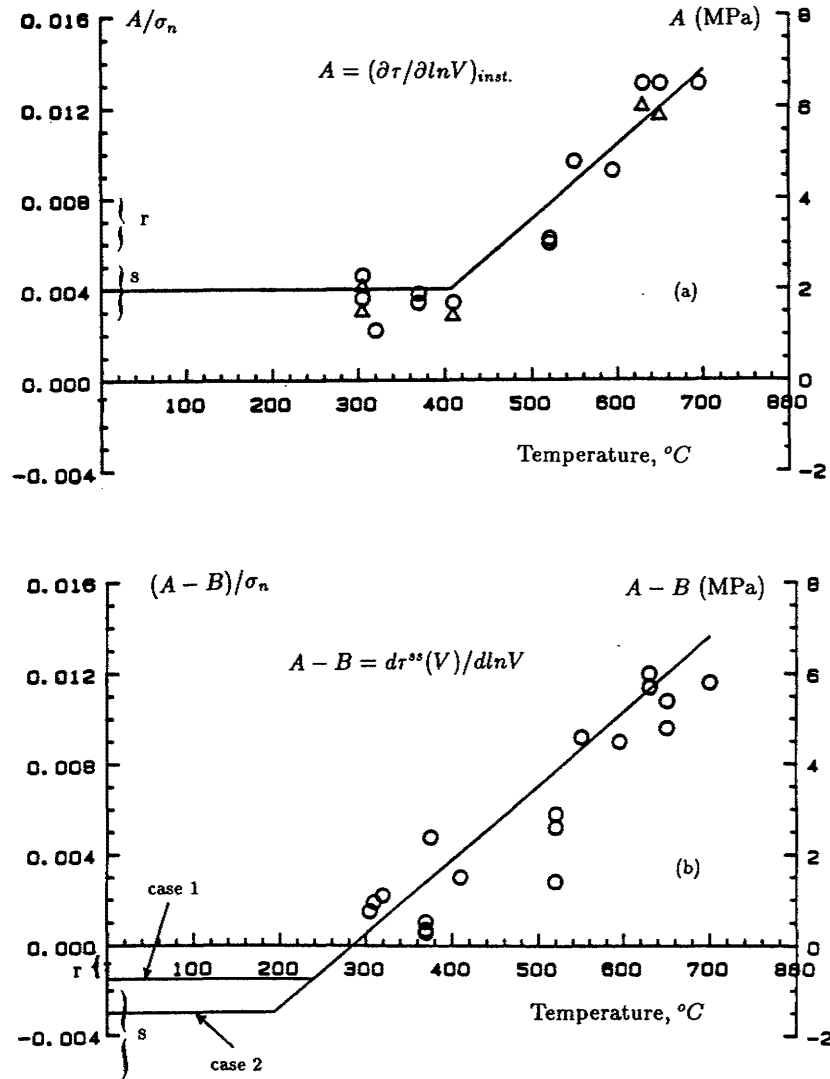
Fig. 1. (a) Temperature variation of instantaneous frictional response, A/σ_n for Westerly granite; (r) and (s) show the ranges of A/σ_n from *Dieterich* [1981] experiments at room temperature for rough and smooth surfaces, respectively. Open circles and triangles are data from *Stesky* [1975] experiments for sudden loading rate increase and decrease, respectively. Solid line is the hypothesized temperature variation of A/σ_n. (b) Temperature variation of long-term frictional response, $(A - B)/\sigma_n$ for Westerly granite; (r) and (s) show the ranges of $(A - B)/\sigma_n$ from *Dieterich* [1981] experiments at room temperature for rough and smooth surfaces, respectively. Open circles are data from *Stesky* [1975] experiments. Solid lines are hypothesized temperature variations of $(A - B)/\sigma_n$. Cases 1 and 2 give ranges for results of *Tullis and Weeks* [1986] at room temperature.

unstable stick slip. Hence as a consequence of the stability analysis described in the introduction, namely, from the result that $d\tau^{ss}(V)/dV(=(A - B)/V) < 0$ leads to possibly unstable slip, depending on the surrounding stiffness and the magnitude of perturbations from steady sliding, it seems appropriate to assume that $(A - B)/\sigma_n$ had turned negative for temperatures below approximately 250°C.

While the adequacy of this conjective and the detailed variations of A/σ_n and $(A - B)/\sigma_n$ with temperature and σ_n remain to be determined by future experiments, one can see the consequences of the data in Figure 1 for sliding on a crustal fault along which temperature increases with depth. The data suggest that sliding at depths for which $T > 300°C$ involves frictional slip with $d\tau^{ss}/dV > 0$ and is inherently stable, at least as judged from the standpoint of single degree of freedom spring-slider systems. By constrast, sliding at shallower depths for which $T < 300°C$, i.e., with $d\tau^{ss}/dV < 0$, involves potentially

unstable frictional response. More generally, we infer a variation of frictional response with depth from a regime with velocity weakening to one with velocity strengthening. It would then seem that the lower limit to the seismogenic depth range can be understood as corresponding approximately to the depth at which this frictional property change takes place. Our more detailed modeling of depth variable strike slip, following *Mavko* [1980, also unpublished manuscript, 1984], certainly supports this contention. Therefore, assuming that the variations with temperature in Figure 1 are representative, one can estimate the seismogenic depth of a crustal fault as the depth at which the temperature is about 300°C.

We will use the San Andreas fault in central California as an example. Suppose both A/σ_n and $(A - B)/\sigma_n$ are fitted linearly for the low- and high-temperature ranges as shown by the solid lines in Figure 1. We are assuming that low-temperature response is essentially temperature independent.
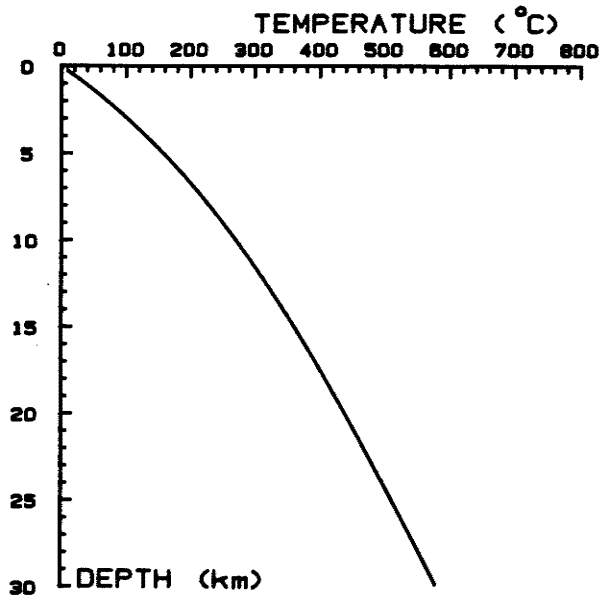
TEMPERATURE (°C)

Fig. 2. A San Andreas fault geotherm from *Lachenbruch and Sass* [1973] (model B in their paper) based on heat flow from the upper mantle and shear heating in the seismogenic zone.

In our present work, we use two possible levels for $(A - B)/\sigma_n$ in the low-temperature range in an attempt to understand the unstable sliding behavior of a fault in relation to the velocity weakening property. These two levels correspond to the lower and upper limits for $(A - B)/\sigma_n$ found in the *Tullis and Weeks* [1986] rotary shear experiments mentioned previously. A system with $(A - B)/\sigma_n$ denoted by case 2 is more brittle (can give larger drops in strength when V increases) than that denoted by case 1. The horizontal line segments fitting to the data in Figure 1 result in the long-term rate sensitivity $A - B$ continuing to be temperature dependent when the instantaneous rate sensitivity A is no longer. Such is not contrary to the data and, in any event, should not be regarded as objectionable since there is evidence that somewhat different physical mechanisms are dominant in the two cases. For example, in comparing slip in a dry argon atmosphere with that in the presence of water vapor, *Dieterich and Conrad* [1984] showed that the long-term rate sensitivity changed sign but the instantaneous rate sensitivity was little altered. Possibly, the instantaneous rate sensitivity is most sensitive to mineral plasticity, whereas the long-term rate sensitivity is also sensitive to surfae adsorption processes which continue to be temperature dependent down to lower temperature. Unless stated otherwise, the case 2 will be used for discussion throughout the paper.

Figure 2 shows a San Andreas fault geotherm derived by *Lachenbruch and Sass* [1973] (model B in their paper) based on the heat flow from the upper mantle and shear heating in the seismogenic zone. The effective normal stress σ_n at depth z km is assumed to be $18z + 10$ MPa (the overburden pressure $28z$ MPa minus the pore pressure $10z$ MPa). In order to facilitate numerical procedures, the threshold normal stress 10 MPa at the earth's surface is chosen so that the viscous response (i.e., A) there is nonzero. This artifact corresponds to adding a layer of soil (about 0.5 km thick) with no friction at the fault trace near the surface. Calculations that have been done both with and without the threshold normal stress are very similar and thus suggest that it has no significant effect on final results. For the reason mentioned earlier, at higher temperature for which temperature-sensitive ductile flow

occurs, A and B are less dependent on, or ultimately independent of, σ_n. For simplicity, we assume that A and B become independent of σ_n at temperature above 407°C (the temperature at which A/σ_n becomes temperature dependent as suggested by the solid line in Figure 1a). Then, one can find the depth variations of A and B (Figure 3). As shown in Figure 3, $A - B$ is then modeled as being negative (potentially unstable slip) along the San Andreas fault down to about 11 km at which the temperature is about 285°C. Also, our fit of the data suggests that B vanishes at depths below 18 km at which the temperature is about 407°C. This means that the long-term rate sensitivity is equal to the instantaneous rate sensitivity. In other words, the frictional response below this depth is slip history independent and thus is simply described as stable nonlinear viscous creep.

The preceding considerations suggest that with the use of the general class of slip rate and slip history dependent friction laws, and notably their consequences for stability of slip, one can predict qualitatively the shallow depth confinement of seismicity of a fault. Nevertheless, the detailed behavior such as how the earthquake instability nucleates or how the friction stress evolves depends on the specific form of the friction law as well as the loading from the surroundings and their elastic stiffness.

Within the class of rate and slip history dependent friction laws, we do further analysis by assuming that for a fixed environment and σ_n, the friction stress τ depends only on V and an evolving phenomenological parameter called a state variable as in previous fits to friction data [*Ruina*, 1980, 1983, 1984; *Gu et al.*, 1984]. Also, we assume that the evolution of the state variable is such that for slip at fixed V, τ evolves exponentially
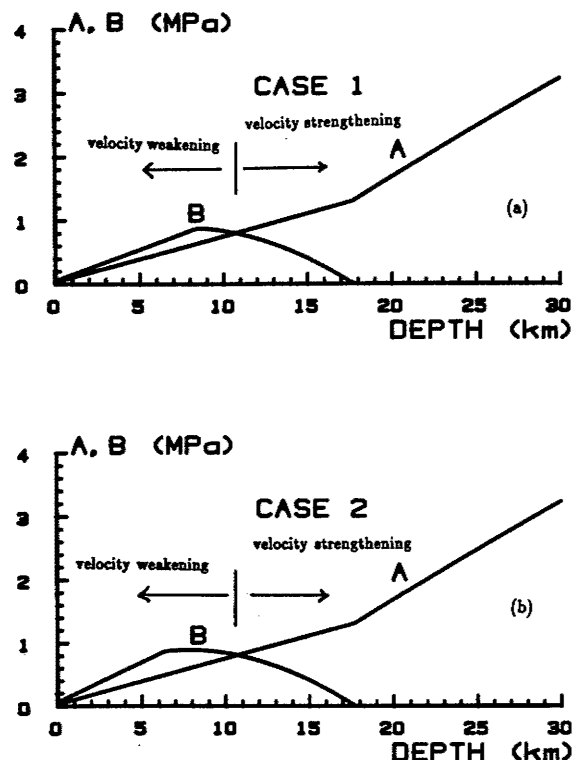

Fig. 3. Depth variations of A and B based on the temperature variations of A and B for (*a*) case 1 and (*b*) case 2, identified in Figure 1, the San Andreas fault geotherm in Figure 2, and assumed normal stress dependence discussed in text.
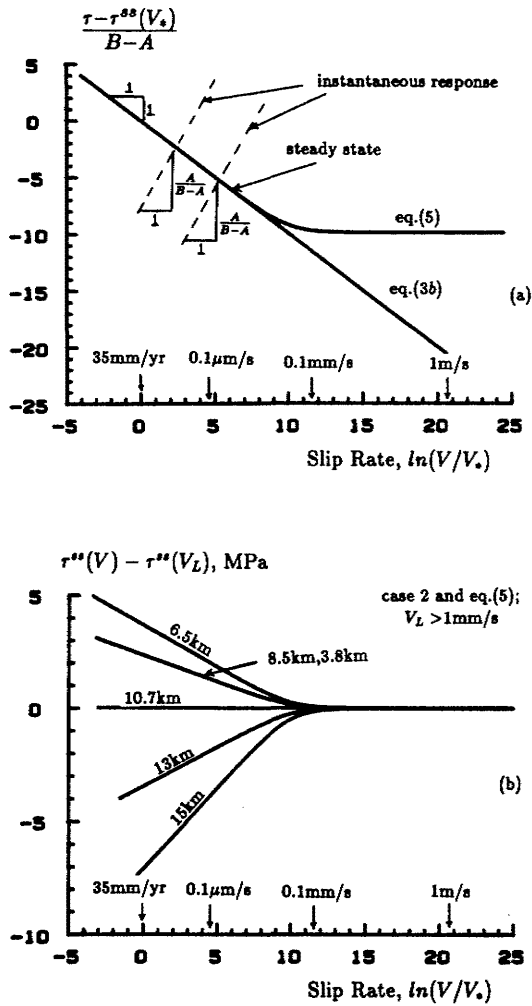
Fig. 4. Velocity dependence of assumed constitutive properties. (a) Instantaneous, dashed lines, and long term (steady state), solid lines, variations of τ with V for shallow portion of crust with velocity weakening, $B - A > 0$. Steady state stress shown with and without high-speed leveling-off option. (b) Variation of steady state strength $\tau^{ss}(V)$ with V for various shallow to midcrustal depths; based on case 2 of Figures 1 and 3, and levelling-off of τ^{ss} above 0.1 mm/s. Here V_L is to be regarded as a seismic slip rate but can be taken (because of leveling) as any value of V above 1 mm/s. Note transition from velocity weakening to strengthening around 11 km. The rate of fall-off of $\tau^{ss}(V)$, with decreasing V, below 11 km increases rapidly with increasing depth and temperature. Since lower depths slip at V on the order of $V_*(=35$ mm/yr) through most of the cycle, this means that large stress increases are needed to achieve seismic slip.

with slip toward its steady state value $\tau^{ss}(V)$ over a characteristic distance L. That is, at fixed V

$$\frac{d\tau}{d\delta} = -\frac{1}{L} [\tau - \tau^{ss}(V)] \qquad (1)$$

where δ is slip. Rice [1983] showed that if the rate of evolution of the state variable is a function of itself and V only, then the foregoing condition serves to define the equation for the evolution rate. In fact, the resulting constitutive relation for general slip history may be written without explicit reference to the state variable at all and is [Rice and Tse, 1986]

$$\frac{d\tau}{dt} = \left(\frac{\partial \tau}{\partial V}\right)_{inst} \frac{dV}{dt} - \frac{V}{L} [\tau - \tau^{ss}(V)] \qquad (2)$$

The specific form of the law will depend on the choice of $(\partial \tau/\partial V)_{inst}$ and $\tau^{ss}(V)$. Within the context of the experiments described earlier, we assume

$$(\partial \tau/\partial V)_{inst} = A/V \qquad (3a)$$

with A constant (for given σ_n and T) and that

$$\tau^{ss}(V) = \tau_* + (A - B) \ln (V/V_*) \qquad (3b)$$

where B is constant also; here V_* is an arbitrarily chosen reference velocity and τ_* is defined such that $\tau^{ss}(V_*) = \tau_*$.

In terms of Ruina's original concept of a state variable θ as a parameter to describe the evolution of the sliding state, with the specific assumption of (3), (2) can be rewritten as

$$\tau = \tau_* + \theta + A \ln (V/V_*)$$

$$\frac{d\theta}{dt} = -\frac{V}{L} [\theta + B \ln (V/V_*)] \qquad (4)$$

These are the equations proposed by Ruina [1980, 1983] as a simplification of a friction law by Dieterich [1981] and which have been employed in several of the stability studies mentioned. For $V_* \simeq 1$ μm/s, τ_*/σ_n is about 0.6, and from Figure 1, A and $A - B$ are only a very small percentage of τ_*. Hence the rate and state dependent friction law described involves a modest departure from the classical concept of a constant stress for sliding friction. However, since as described earlier that stability of steady state sliding depends on $d\tau^{ss}/dV$, this small variation is critical in determining whether slip is stable or not. In other words, stability is related to the relative change in stress rather than the absolute level of stress.

In experiments done by Scholz and Engelder [1976] and Dieterich [1978] on the same type of rocks as considered above, it is found that while τ^{ss} has the simple linear relationship of (3b) with the logarithm of V at low speeds, τ^{ss} tends to become independent of V at higher speeds (above 0.1 mm/s in results of Dieterich [1978]). Hence another similar form of constitutive relation that seems to be consistent with the high speed phenomena would be written as

$$\tau^{ss}(V) = \tau_* - (A - B) \ln (V_*/V + e^{-n}) \qquad (5)$$

Here n is a positive number chosen (depending on the choice of reference speed V_*) in such a way that $\tau^{ss}(V)$ reduces to a residual level when the slip speed is above a certain value. For example, with $V_* = 35$ mm/yr (typical relative slip rate along the creeping portion of the San Andreas fault), n can be taken as 10 to cause $\tau^{ss}(V)$ is to level off in the vicinity of 0.1 mm/s. We use this value in our depth variable slip simulations when we use (5) rather than (3b) in (2).

We note that no feature of the earthquake cycles that we analyze is dependent on either the magnitude or depth variation of τ_*, the strength for steady slip at the reference speed. Rather, all characteristics of the simulated cycles are determined by the constitutive parameters A and $A - B$, which measure sensitivity of strength to changes in velocity, and by the relaxation slip L; L is not well constrained, and its effect in the simulations is considered subsequently.

Figure 4 summarizes the velocity dependence of properties assumed for our subsequent simulations. In Figure 4a the dashed lines show how stress varies with a rapid (instantaneous) variation in slip velocity. However, as slip accumulates, the stress continually evolves (following (2) and (3a)) toward the steady state value $\tau^{ss}(V)$ appropriate to the then current V.
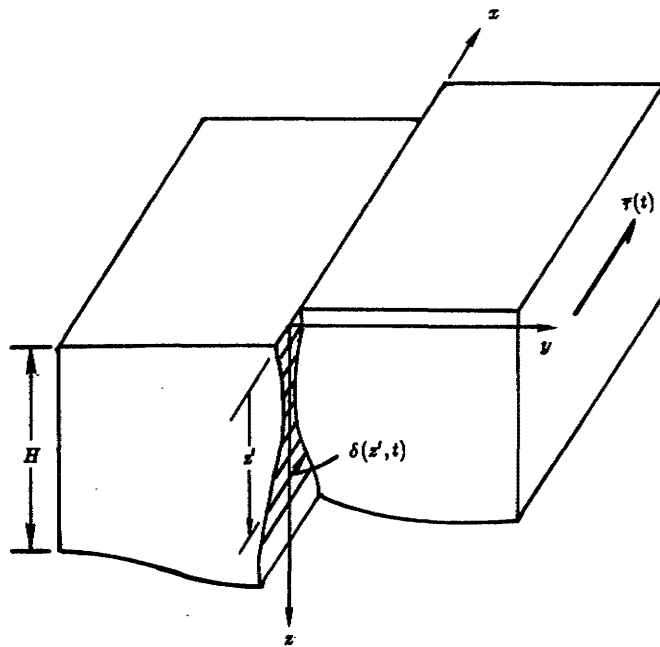
Fig. 5. Local cross section of the fault showing the depth variable slip. $\bar{\tau}(t)$ is the thickness averaged shear stress transmitted across the fault surface.

The two choices we use for the steady state strength variation, given by (3b) and (5), are shown as solid lines. Those have been drawn with the negative slope appropriate to the relatively cool shallow crust, above 11 km, where the friction is of a potentially unstable type with velocity weakening.

For Figure 4b the $A - B$ variation denoted by case 2 in Figures 1b and 3b is adopted, together with the leveling-off of τ^{ss} at high V as in (5). Figure 4b shows the assumed variation of $\tau^{ss}(V)$ with V at several crustal depths. The shallow depths show velocity weakening, which is greatest at 6.5 km depth (it is greatest at 8.5 km for case 1), and prevails to about 11 km where velocity strengthening takes over with further increase of depth. The fall-off of τ^{ss} with decreasing V becomes more abrupt as we go to greater and hotter depths. The laboratory data leading to the supposed linear variation of τ^{ss} (V) with ln V shown in Figure 4 extends from V of 100 μm/s (0.1 mm/s) down to 0.1 μm/s both marked on Figure 4, for the high-temperature data; some of the room temperature data extends to 0.01 μm/s. (In our use of (5) rather than (3b), we actually level off τ^{ss} before reaching 100 μm/s.) As Figure 4b shows, we are assuming without evidence that the linear variation with ln V extends down to V of order 0.001 μm/s (30 mm/yr), i.e., comparable to the plate velocity $V_* = 35$ mm/yr, also marked on Figure 4 and below.

Our simulation of earthquake cycles to follow shows that the depth ranges below 11 km with velocity strengthening essentially slip at speeds of order V_* throughout most of the cycle. Thus Figure 4b shows that those depth ranges are stressed below the stress level required for rapid seismic depth. It is this relaxation of prevailing stress below the seismic level, which becomes more pronounced with increasing depth, that causes the shallow depth confinement of seismicity. Even the major stress transfers to the deeper part of the fault zone, from the great ruptures of the velocity weakening zone above the 11-km transition depth, are then inadequate to cause seismic stress levels to be reached over more than a few kilometers

below the transition depth. We emphasize that the shallow depth confinement of seismicity is thus consistent with deformation localization to a fault extending well below the seismogenic zone; it does not require an assumption that the seismically active fault zone be underlain by a zone of broadly distributed creep deformations.

Of course, our depth variable constitutive model suffers from the paucity of data and lack of precise knowledge of fault zone structure and composition. However, to the extent that it at least qualitatively incorporates the variation of fault constitutive response with depth, and assuming localization of deformation to a fault penetrating deeply into the crust, we may expect the verbal description of depth confinement given above and the quantitative earthquake mechanics simulations which follow to be reasonable analogues of the great strike slip earthquake process.

Figure 4b should not be understood as implying that $\tau^{ss}(V_L)$ for a rapid (seismic) slip rate V_L is the same for all depths. However, whether it is or not is irrelevant to all aspects of the earthquake cycle that we describe. Our results depend only on how τ varies with V (and its history) at each depth, since that is what determines the nature of slip throughout the crust and its instability. The results have no dependence whatever on how τ varies with depth at a fixed V (or V history), and it is to some extent curious that this latter issue has received so much attention relative to the former in the existing literature. The latter issue would be critical, however, to an extension of the present studies which sought for consistency to quantify the contribution of such shear deformations as we predict to the temperature distribution with depth.

Future experiments may reveal a much richer structure than assumed here in variation of $\tau^{ss}(V)$ with V and normal stress. For example, using halite gouge between intact sandstone as a room temperature analogue for hotter crustal fault zone materials, *Shimamoto and Logan* [1986] found that high normal stress tests showed velocity stengthening for all V studied, from about 0.01 to 1000 μm/s. However, at low normal stress (50 MPa confining pressure) they found velocity strengthening below 0.01 μm/s, weakening from 0.01 μm/s to 10 μm/s, and strengthening again above 10 μm/s.

Modeling of Crustal Earthquake Instability

In this section a strike-slip fault model like that of *Mavko* [1980, also unpublished manuscript, 1984] based on the friction law (2) with (3a), and (3b) or (5), but with our estimated depth dependence of friction parameters (e.g., A and B as shown in Figure 3), is used to calculate the depth and time variations of slip at a plate margin over several earthquake cycles. Results confirm the expected depth confinement of seismicity to the shallow crust and show additional features such as the nucleation of instabilities, regain of fault strength or formation of effectively locked patches after earthquakes, etc.

The lithosphere is assumed to be a homogeneous linear elastic plate of thickness H cut along the fault zone as in Figure 5. The top and bottom surfaces of the plate are shown as stress free. That condition on the bottom face corresponds to decoupling of the lithosphere from the viscous asthenospheric foundation and is justified only if the asthenosphere is completely relaxed. Nevertheless, a mathematical formulation for the coupling of the lithospheric plate to a viscoelastic asthenosphere is possible within this type of model; *Li and Rice*
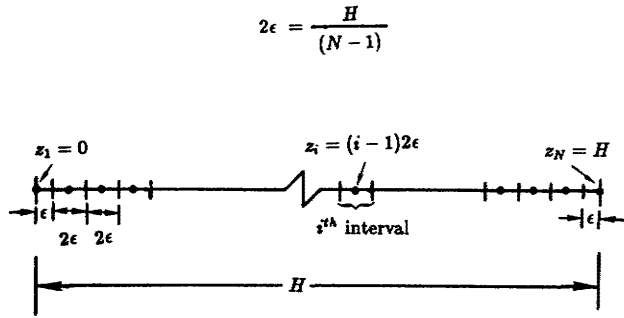
$$2\epsilon = \frac{H}{(N-1)}$$

Fig. 6. A diagram showing the discretized plate.

[1983] gave an extensive discussion of the formulation procedures. As we are at this point interested in understanding the depth variation of fault response, we approximate the actual three-dimensional situation by treating the depth variation of stress and slip as if they were the same at each section along the fault trace $(-X < x < X)$. Actual finite extent of the active fault segment along strike and the coupling of the lithospheric plates to the asthenosphere may be incorporated approximately by requiring that the thickness averages of stress $\bar{\tau}(t)$ and slip $\bar{\delta}(t)$ at the plate margin be related to one another in a manner that is consistent with those features. This is expressed mathematically by writing

$$\bar{\tau}(t) = \bar{\tau}_0 + \int_{-\infty}^{t} k_0(t - t')\left[V_{pl} - \frac{d\bar{\delta}(t')}{dt'} \right] dt' \qquad (6a)$$

where $\bar{\tau}_0$ is a constant, the value of which is irrelevant to our simulations of earthquake cycles, V_{pl} is the average plate velocity accommodated by the fault zone over many earthquake cycles, and $k_0(t)$ is a time dependent stiffness which can be estimated as discussed by *Li and Rice* [1983] (who actually use the time dependent compliance that is inverse to $k_0(t)$). The equation expresses the idea that it is the mismath between V_{pl} and $d\bar{\delta}/dt$ which causes the force transmitted across the lithospheric fault zone to accumulate or drop. From *Li and Rice* [1983, equations (14) and (15)], the long time value corresponding to complete relaxation of the asthenosphere is $k_0(\infty) = k = \mu\pi(1 + v)/8X$, where μ and v are the shear modulus and Poisson's ratio, respectively. As an approximation we neglect the time dependence of coupling to the asthenosphere, treating it as relaxed for all time so that $k_0(t) \simeq k$ and absorb the constant above into the origin for the time axis so that (6a) becomes

$$\bar{\tau}(t) = k[V_{pl}t - \bar{\delta}(t)] = \frac{\mu\pi(1 + v)}{8X}[V_{pl}t - \bar{\delta}(t)] \qquad (6b)$$

With $\mu = 3 \times 10^4$ MPa, $v = 0.25$, and $X = 180$ km, this gives $kV_{pl} = 3 \times 10^{-3}$ MPa/yr for the nominal lithosphere average stress accumulation rate in the absence of relaxation by slip at the boundary. According to limited trial calculations, features of the subsequently reported earthquake cycles have essentially negligible change when X is reduced (or k increased) by a factor of 3.

The local depth variable stress $\tau(z, t)$ at the fault trace can be written as a uniform part, equal to $\bar{\tau}(t)$ of (6), plus an additional portion (averaging to zero over the plate thickness) due to the nonuniformity of local slip $\delta(z, t)$. That is,

$$\tau(z, t) = \bar{\tau}(t) - \int_0^H G(z, z') \frac{\partial\delta(z', t)}{\partial z'} dz' \qquad (7a)$$

where

$$G(z, z') = \frac{\mu}{4H}\left[\frac{\sin\dfrac{\pi z'}{H}}{\sin\dfrac{\pi(z - z')}{2H}\sin\dfrac{\pi(z + z')}{2H}} \right] \qquad (7b)$$

is the Green's function which gives the shear stress at depth z induced by a unit screw dislocation at depth z'. The derivation of this Green's function and other related formulae are given in the appendix.

Equivalently, the local depth variable stress $\tau(z, t)$ can be represented by

$$\tau(z, t) = \bar{\tau}(t) - \frac{\mu}{2\pi}\int_{-\infty}^{\infty} \frac{1}{z - z'}\frac{\partial\delta(z', t)}{\partial z'} dz' \qquad (8)$$

where $\delta(z, t)$ here is defined outside $0 < z < H$ so as to be periodic in z with a period of $2H$, and symmetric about $z = 0$ and $z = H$, so that the traction free boundary conditions at the earth's surface and the bottom of the lithosphere are satisfied. The stress $\tau(z, t)$ is also periodic with the same period $2H$ and the calculated stress for the range $z = 0$ to $z = H$ would be identical to that calculated from (7). Due to the periodicity of $\delta(z, t)$, the convolution integral in (8) can be calculated using Fourier methods; that is, the integral in the space domain becomes multiplication in the frequency domain, and the result is converted back into the space domain. Numerically, the process is performed efficiently by the fast Fourier transform (FFT) method, which is generally faster than solving the integral term in (7a) using matrix multiplication in the discretized version of the integral. However, when the stress distribution is known instead of the slip distribution or when partial slip or stress distribution is known (as will be seen later, during the earthquake instability only the stress drop in the seismically rupturing region and the slip in the region below is known), FFT is not convenient to use. Hence we develop a solution method, which will be used when the above case occurs, for the singular integral term in (7a).

The plate thickness H is divided into N intervals as shown in Figure 6 such that the first and last intervals are of length ε ($= H/2(N - 1)$), while the remaining intervals are of equal length 2ε. In each of these intervals the slip is assumed to be uniform for the purpose of calculating the shear stress at the center of any interval (or at the surfaces of the plate) so that stress and slip can be related to one another by the constitutive relations. For FFT this corresponds to the discretization of half of the wavelength of the quantity and the other half can easily be generated using the symmetry at $z = H$. Hence using the Green's function in (7b), the shear stress at z_i, depth of the midpoint of interval i, due to uniform slip δ_j in interval j is given by $k_{ij}\delta_j$, where

$$k_{ij} = G(z_i, z_j - \varepsilon) - G(z_i, z_j + \varepsilon) \qquad j \neq 1, N$$
$$k_{i1} = -G(z_i, \varepsilon) \qquad k_{iN} = G(z_i, H - \varepsilon) \qquad (9)$$

For slip distribution over the thickness H (i.e., N intervals) the dislocation contribution to shear stress at z_i is $\sum_{j=1}^{N} k_{ij}\delta_j$. As suggested earlier, this vanishes when δ is uniform. Also, in a discretized form the thickness average of any quantity (e.g., $\bar{\delta}(t)$) can be written as

$$\bar{\delta}(t) = \frac{1}{H}\int_0^H \delta(z, t)\, dz = \frac{1}{H}\left[\sum_{i=2}^{N-1} \delta_i 2\varepsilon + (\delta_1 + \delta_N)\varepsilon \right]$$

or

$$\delta(t) = \frac{1}{N-1}\left[\sum_{i=1}^{N} \delta_i - \frac{\delta_1 + \delta_N}{2}\right]$$

Then, together with (6b), the equilibrium equation (7a) is discretized as

$$\tau_i(t) \equiv \tau(z_i, t) = kV_{pl}t - \sum_{j=1}^{N} K_{ij}\delta_j(t) \qquad (10a)$$

where

$$K_{ij} = k_{ij} + \frac{\mu\pi(1+\nu)}{8X}\frac{1}{N-1} \qquad j \neq 1, N \qquad (10b)$$

$$K_{ij} = k_{ij} + \frac{\mu\pi(1+\nu)}{16X}\frac{1}{N-1} \qquad j = 1 \text{ or } N \qquad (10c)$$

The time derivative of $\tau_i(t)$ is

$$\frac{d\tau_i(t)}{dt} = kV_{pl} - \sum_{j=1}^{N} K_{ij}V_j(t) = \sum_{j=1}^{N} K_{ij}[V_{pl} - V_j(t)] \qquad (11)$$

The general constitutive law (2) for the fault is conveniently written as

$$\frac{d\tau_i(t)}{dt} = \frac{A_i}{V_i(t)}\frac{dV_i(t)}{dt} - \frac{V_i(t)}{L_i}\{\tau_i(t) - \tau_i^{ss}[V_i(t)]\} \qquad (12)$$

It should be understood that $(\ )_i$ denotes $(\ )$ at depth z_i. Hence together with specific forms of A_i and $\tau_i^{ss}(V)$, equations (11) and (12) constitute a system of first-order nonlinear ordinary differential equations in V_i and τ_i whose solution can be sought once appropriate initial conditions for V and τ are prescribed. The slip distribution is then found from inversion of (10a). FFT is used for efficiency in the numerical iterative process of solving the differential equations (11) and (12). In general, the velocity and stress distributions in a fault at any stage of sliding are not known a priori. However, we find in our simulations that the fault surface ultimately evolves toward periodic earthquake cycles (more complicated friction laws might lead to aperiodic cycles). To hasten this evolution, we choose an initial condition to represent approximately a fault that has just gone through an earthquake and is ready to start a new cycle. The stress distribution is taken as steady state values appropriate to the expected seismogenic layer (depth over which $A - B$ is negative or slightly extending into the region where $A - B$ is positive due to possible overshoot) sliding at a high seismic particle slip speed V_L (taken as about 1 m/s) while the slipping rate below decreases to the relative plate velocity V_{pl} at the bottom. The results show that the earthquake cycle seems to become periodic after a few cycles, losing memory of the artificial initial condition.

Finally, it should be noted that the quasi-static analysis presented so far has ignored the effect of inertia. Hence slipping at some depth (or some region in a discretized form) is said to become unstable when the slip rate becomes unbounded. In the case of a single degree of freedom system, Dieterich [1978, 1980] introduced a limiting speed procedure; it was also adopted by Mavko [1980, also unpublished manuscript, 1984] for the continuum case. In that procedure, once a limiting speed V_L is reached at a given location, slip there is assumed to continue at speed V_L, and the stress there as estimated from quasi-static elastic analysis (as by (10a) for the continuous system) is no longer required to equal that calculated from the constitutive relation (i.e., from (12) in the pres-

ent case). The latter rapidly approaches $\tau^{ss}(V_L)$ in typical circumstances for which the rapid slip is much greater than L. Quasi-static calculations resume (i.e., equality between the stresses of (10a) and (12) is reestablished) when enough high-speed slip accumulates such that τ estimated from (10a) reduces to that given by (12), i.e., effectively $\tau^{ss}(V_L)$. Rice and Tse [1986] showed how to modify this limiting speed procedure for a single degree of freedom system so as to include dynamic overshoot. They resume quasi-static calculations when τ as calculated from elastic considerations reduces to a prescribed value $\tau^{(2)}$ below $\tau^{ss}(V_L)$. The velocity $V^{(2)}$ at which quasi-static calculations resume is that appropriate to rapid (instantaneous, at fixed state) reduction of stress from $\tau^{ss}(V_L)$, the value during rapid slip, to $\tau^{(2)}$ during the arrest of seismic motion. Thus for A constant one finds from (3a) that

$$V^{(2)} = V_L \exp\{-[\tau^{ss}(V_L) - \tau^{(2)}]/A\} \qquad (13)$$

Rice and Tse [1986] show that this modified limiting speed procedure can closely reproduce results of a full analysis including inertia for the single degree of freedom system provided the overshoot $\tau^{ss}(V_L) - \tau^{(2)}$ is chosen as approximately 90% of the stress drop $\tau^{(1)} - \tau^{ss}(V_L)$, where $\tau^{(1)}$ is the stress calculated according to the quasi-static analysis when the limiting speed is first attained.

Unfortunately, our attempts to adapt the limiting speed procedure to the continuous case considered in this paper suggest that an extremely small grid size is required to model sensibly the bilateral, cracklike spread of rupture from the grid location where V_L is first reached. This requires a large amount of computer time which is difficult to justify given the neglect of inertia in the procedure. Further, our modification of the limiting speed procedure [Rice and Tse, 1986] so as to include dynamic overshoot is not readily applied to the present case, at least for the range of grid sizes that we can regard as computationally feasible; difficulties with it relate to the fact that the grid points tend to reach limiting speed, slip, reduce their stress, and arrest according to the procedure before neighboring points go unstable.

We have therefore adopted the following approach to dealing with the slip once any one element of our grid reaches V_L. We assume that a rupture event begins at that location and spreads rapidly over a certain set of neighboring grid elements, whose exact extent is determined by trial and error calculations as described later. Let the indices i of all grid elements which partake in the seismic slip be denoted by the set $\{i(s)\}$. The stress distribution $\tau_i^{(1)}$ is known from the numerical calculation based on (10)–(12) at the beginning of the seismic slip, and we assume that the stress $\tau_i^{(2)}$ immediately after can be prescribed for all i included in $\{i(s)\}$. For example, $\tau_i^{(2)} = \tau_i^{ss}(V_L)$ in the absence of dynamic overshoot, and $\tau_i^{ss}(V_L) - \tau_i^{(2)}$ is chosen as some given fraction (say, 20–30%) of $\tau_i^{(1)} - \tau_i^{ss}(V_L)$ when overshoot is taken into account.

We need to calculate the slip $\delta_i^{(2)} - \delta_i^{(1)}$ during the seismic event; this is assumed to be zero for i outside of the set $\{i(s)\}$ and is calculated for i in $\{i(s)\}$ by writing from (10) that

$$\tau_i^{(1)} - \tau_i^{(2)} = \sum_{j \in \{i(s)\}} K_{ij}[\delta_j^{(2)} - \delta_j^{(1)}] \qquad i \in \{i(s)\} \qquad (14)$$

Hence inversion of the submatrix of $[K]$ indicated gives the seismic slip. The same relation as above then lets one calculate the stress $\tau_i^{(2)}$ immediately after the seismic event at locations i outside the set $\{i(s)\}$. The quasi-static calculation based on (11)

TABLE 1. Summary of Some of the Earthquake Cycle Parameters for Different Simulations Discussed in the Text

		Surface Slip, m		Depth, km		Cycle Time, years
Case*	Figure Number	Total	Coseismic†	Initiation	Rupture Extent	
C2L40L00	7	2.95	1.90	6.7	13.9	84
C2L40L30	10	3.25	2.57	6.7	15.2	93
C2L40N00	12	4.35	3.49	2.8	13.8	124
C2L40N30	13	5.56	4.79	4.2	15.1	159
C2L10L00	14	2.29	1.74	4.6	13.8	65
C2L10L30	15	2.79	2.45	5.4	15.1	80
C1L40L00	16	2.13	0.83	7.2	13.3	61
C1L40L30	17	2.24	1.13	7.2	14.2	64

*For example, C2L40L00: case 2, $L = 40$ mm, leveling off of steady state stress at high speed (i.e., equation (5)) and no dynamic overshoot in stress and C2L40N30: case 2, $L = 40$ mm, no leveling off of steady state stress (i.e., equation (3b)) and 30% dynamic overshoot in stress.

†Includes only the "instantaneous" slip; in some simulations, particularly those without dynamic overshoot, significant additional slip accumulates in a few seconds (e.g., Figures 7, 14, 16, and 17).

and (12) then resumes with the suddenly altered stress distribution $\tau_i^{(2)}$ and velocity distribution $V_i^{(2)}$, the latter given by

$$V_i^{(2)} = V_L \exp\{-[\tau_i^{ss}(V_L) - \tau_i^{(2)}]/A_i\} \qquad i \in \{i(s)\}$$
$$V_i^{(2)} = V_i^{(1)} \exp\{[\tau_i^{(2)} - \tau_i^{(1)}]/A_i\} \qquad i \notin [i(s)] \tag{15}$$

The trial and error procedure necessary to estimate $\{i(s)\}$ is carried out as follows. For a true continuum the sudden slip zone would have to extend deep enough that the stress "drop" over part of the rupture zone was negative (see, e.g., *Walsh* [1968] and *Burridge and Halliday* [1971]) and no crack-tip-like stress singularity results at the border of that zone. In the discretized numerical procedure we let the rupture penetrate into the zone where the stress drop would be negative (that is, slightly into the hotter region where $d\tau^{ss}(V)/dV$ is positive) until, by trial calculations, we have established a depth at which the stress drop is, within limits of numerical discretization, apparently continuous across the border of the zone. That is, we locate the depth at which there is no abrupt variation of stress alteration $\tau_i^{(2)} - \tau_i^{(1)}$ at border of set $\{i(s)\}$.

For a single degree of freedom system the procedure adopted here is identical to the *Rice and Tse* [1986] limiting speed procedure as discussed above. For the continuous system it eliminates the modeling of slip propagation through the grid, which is costly in terms of computer time and would presumably require an extremely small grid size (scaling with slip decay distance L) for simulation of cracklike spreading of the slip zone and is of questionable accuracy due to neglect of inertia.

The procedure outlined also lets us explore the effect of a wide range of values for L. This parameter is thought to scale in some as yet not well characterized way with the roughness scale of the surface [*Dieterich*, 1981]. Laboratory friction experiments suggest values in the range of 10^{-5} to 10^{-4} m. However, if we assume that L can be equated to critical slip weakening distances in a slip-weakening fracture model and use estimates of critical fracture energy for nucleation of large earthquakes by crack like stress concentration from slip below a locked seismogenic zone [*Li and Rice*, 1983; *Rice*, 1983], then estimates of L in the range 10^{-2} to 10^{-1} m result. Within the storage capability on the Cray I computer and computational feasibility in our work, a range of values of L is used

in the numerical simulations and the results are reported in the next section.

RESULTS AND DISCUSSIONS

Using the parameters described earlier and the depth distributions of A and B (case 1 or case 2 as shown in Figure 3), many simulations of earthquake sequences have been done for different choices of the form of the steady state stress law (equation (3b) or (5)), inclusion or noninclusion of dynamic overshoot in stress (last section), and magnitude of the characteristic slip distance L. Since the global features and mechanical processes in all cases are similar, as an illustration we will discuss in detail the earthquake simulation only for case 2 with $L = 40$ mm, no inclusion of dynamic overshoot, and with a steady state strength independent of velocity at slip rate above 0.1 mm/s, i.e., (5). This simulation is coded C2L40L00; see Table 1 for explanation. Variations from this case can be made by including dynamic overshoot in stress (e.g., 30%), by using a different steady state stress law (e.g., equation (3b)), by using case 1 (i.e., less brittle), or by using a smaller value of L. A more extensive presentation of numerical results is given by *Tse* [1985].

In the context of the discussion of frictional response, the expected seismogenic depth is approximately the transition depth at which the frictional response changes from velocity weakening ($d\tau^{ss}/dV < 0$) to velocity strengthening ($d\tau^{ss}/dV > 0$). With the present distributions of A and B, this depth is about 11 km. The simulations confirm the importance of this transition depth in separating zones of qualitatively different response. Much of the zone above 11 km slips very slowly and is effectively locked through most of the cycle, whereas the deeper zone slips continually. Near the end of the effectively locked period, the slip rate and the stress in the stable region below are slightly lower than the relative plate velocity V_{pl} and the corresponding steady state stress level $\tau^{ss}(V_{pl})$, respectively, while the stress in the nearly locked zone has increased to a level generally above the steady state stress $\tau^{ss}(V_{pl})$ that is needed to slide steadily at the relative plate velocity (35 mm/yr.) Somewhere in this locked zone a small region, the size of which increases with the magnitude of the characteristic slip distance L, begins to unload itself. The stress there decreases, and local slip takes place with increasing speed. For L sufficiently large so that the stress can be relaxed only over a large slip distance, this stress-unloading region expands, and the whole seismogenic zone undergoes stress reduction stably, i.e., without an earthquake. In the current case (case 2), stable episodic slip relieving stress in the locked zone is observed for L between about 80 mm and 160 mm; the fault surface slides steadily at V_{pl} over the entire depth range for L above 160 mm. However, if L is small enough (below 80 mm in the present case), such that stress relaxation can be accomplished over only a small slip distance, the unloading process that begins in this small zone leads to an accelerating slip velocity and significantly concentrates stress onto neighboring regions above and below which then slip at an accelerating rate too so that a great earthquake instability spreads over the previously locked zone.

During the instability the stress in the previously locked zone is at a lower level associated with high sliding speed V_L, and hence an increase of stress is transferred to the stable region below. As mentioned earlier, this causes the coseismic rupture zone to penetrate beyond 11 km depth, into the region where the frictional response is velocity strengthening. Typi-

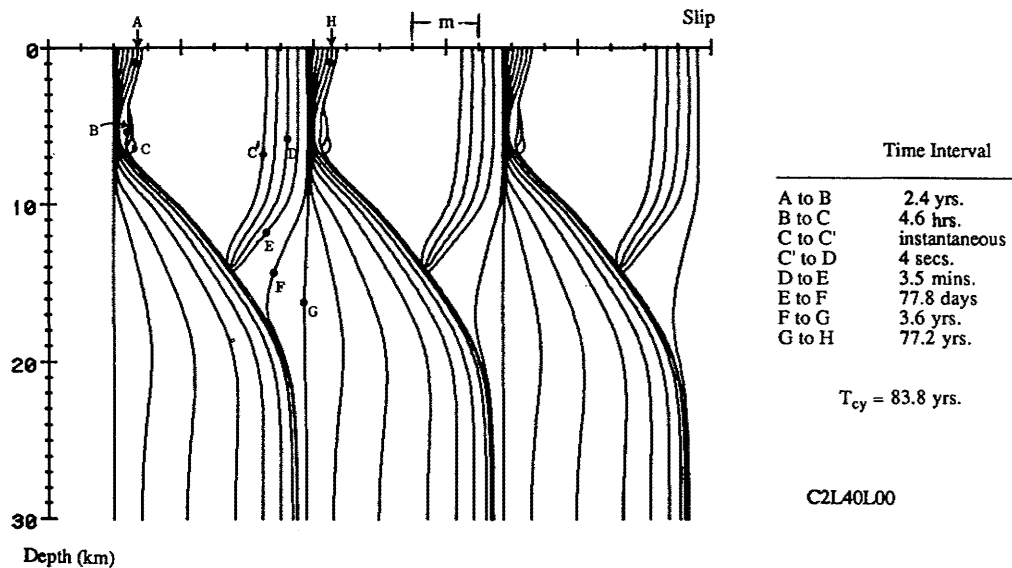| Time Interval	
A to B	2.4 yrs.
B to C	4.6 hrs.
C to C'	instantaneous
C' to D	4 secs.
D to E	3.5 mins.
E to F	77.8 days
F to G	3.6 yrs.
G to H	77.2 yrs.

$T_{cy} = 83.8$ yrs.

C2L40L00

Fig. 7. Plot of slip vs depth through a time history of three earthquake cycles. The simulation is based on the steady state stress law (5), such that the steady state stress becomes velocity independent when velocity is above 0.1 mm/s, and $L = 40$ mm; dynamic overshoot in stress is not included. Depth distributions of A and B are denoted by case 2 in Figures 1 and 3. Other parameters used for the calculation are indicated in the text. This simulation is coded C2L40L00; see Table 1 for explanation. Each line represents a constant time, but the time interval between any two adajacent lines is not uniform. The time intervals between some representative lines are indicated.

cally, the coseismic slip tapers off to zero at 13–15 km depth, although rapid postseismic slip occurs over a further 3–4 km depth.

For the simulation C2L40L00 based on case 2 with $L = 40$ mm, no inclusion of dynamic overshoot and steady state stress independent of velcoity at slip rate above 0.1 mm/s (Figure 7), the rupture initiates at about 7 km and extends to about 14 km (about 3 km below the transition depth). After the instability the stress relaxation and the decrease in slip rate in the rupture zone continue. In less than a year the slip rate in the rupture zone becomes low enough that an effectively locked patch, which roughly extends from near the transition depth to the earth's surface, is reestablished. At the same time, rapid postseismic creep occurs below the rupture zone and penetrates down to about 18 km; this continues at a noticeably

higher rate for about 4 years after the earthquake. The ductile region at greater depths seems to be only modestly perturbed by the earthquake occurring above and continues to slide relatively steadily at about the relative plate velocity. During the period that the seismogenic layer is effectively locked, the continuing tectonic plate motion increases the shear force transmitted across the fault zone, and stress is further concentrated onto the effectively locked zone by the continual slip below. Thus the locked region is gradually eroded from below leading to accelerating preseismic slip and finally earthquake instability again. The general picture of the earthquake cycle predicted by these calculations seem broadly consistent with the phenomenology of earthquakes along the San Andreas fault system.

Figure 7 shows the slip versus depth through a time history

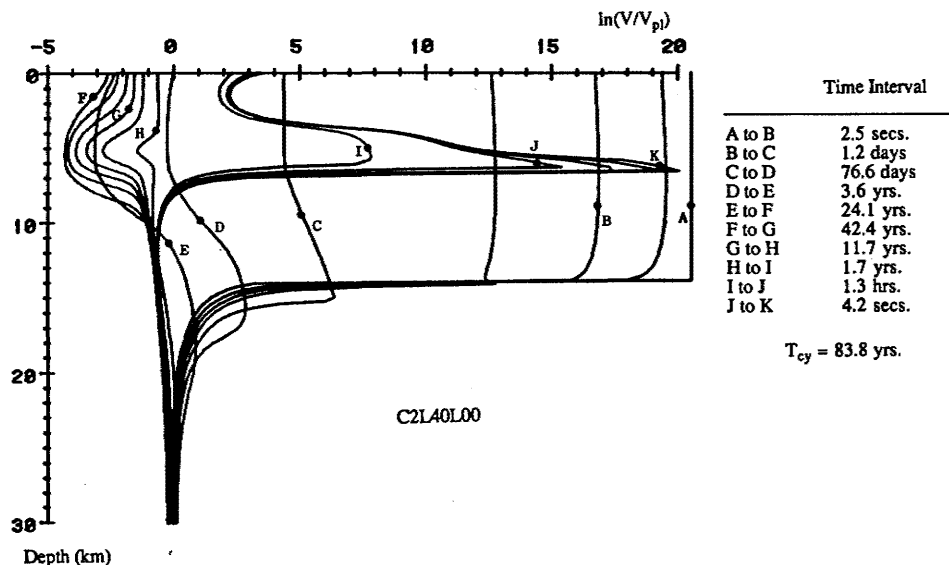| Time Interval	
A to B	2.5 secs.
B to C	1.2 days
C to D	76.6 days
D to E	3.6 yrs.
E to F	24.1 yrs.
F to G	42.4 yrs.
G to H	11.7 yrs.
H to I	1.7 yrs.
I to J	1.3 hrs.
J to K	4.2 secs.

$T_{cy} = 83.8$ yrs.

C2L40L00

Fig. 8. Plot of logarithm of normalized slip rate versus depth for simulation of Figure 7 (C2L40L00). Each line represents a constant time, and time intervals between some lines are indicated.
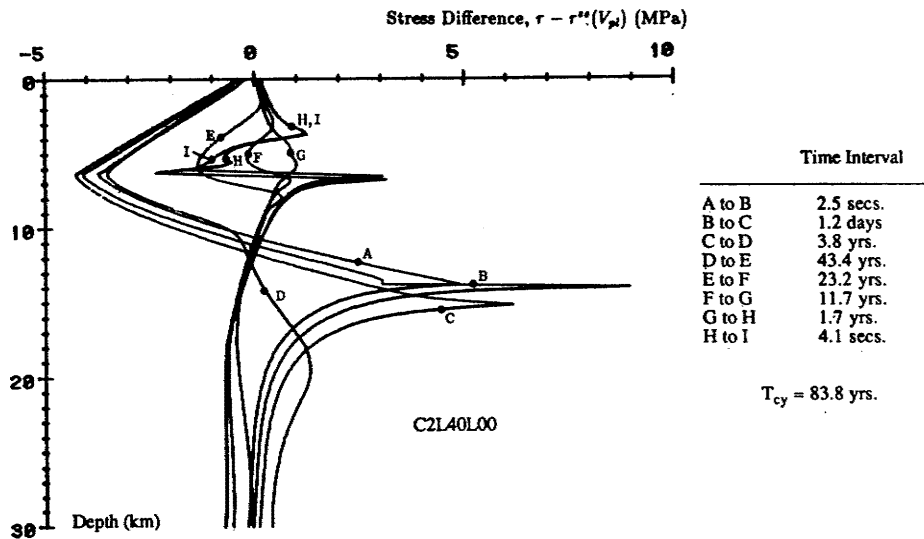
Stress Difference, $\tau - \tau^{ss}(V_{pl})$ (MPa)

Time Interval	
A to B	2.5 secs.
B to C	1.2 days
C to D	3.8 yrs.
D to E	43.4 yrs.
E to F	23.2 yrs.
F to G	11.7 yrs.
G to H	1.7 yrs.
H to I	4.1 secs.

$T_{cy} = 83.8$ yrs.

C2L40L00

Fig. 9. Plot of stress difference (stress minus steady state stress at the relative plate velocity, $V_{pl} = 35$ mm/yr) versus depth for simulation of Figure 7 (C2L40L00). Each line represents a constant time, and time intervals between some lines are indicated.

of three earthquake cycles. The cycles seem to repeat one after the other. Each line represents a constant time, but the time interval between any two adjacent lines is not uniform. Time intervals are marked at the margin of Figure 7. That marked "instantaneous" from C to C', corresponds to the coseismic slip, although some subsequent slip (C' to D) accumulates so rapidly that it too should be considered as coseismic. As one can see from (10a), the initial slip distribution with depth can be chosen arbitrarily. In the presentations here it is chosen to be uniform with depth approximately 5 years after the earthquake, when the rapid postseisimic slip at the base of the seismic rupture is more or less completed. The time interval between A and H is equal to 84 years, which is the cycle time for an earthquake in this simulation. Figure 7 shows that a fraction of the total slip is accomplished aseismically near the earth's surface during the later part of the earthquake cycle. As will be seen later, this near-surface slip and associated stress relaxation increases with decreasing magnitude of

$A - B$ in the shallow crust and increases with the characteristic slip distance L.

Figure 8 shows the logarithm of the normalized slip rate versus depth. As mentioned above, in less than a year the rupture zone has slowed down, and postseismic creep extends to about 18 km (lines D and E). The rupture initiates at about 7 km, near which $B - A$ is maximum (Figure 3b). Figure 9 shows the stress difference $\tau - \tau^{ss}(V_{pl})$ (stress minus the steady state stress for sliding at the relative plate velocity) versus depth. Near the end of the effectively locked period (line G), the stress in the seismogenic zone is above while the stress in the ductile zone is below the steady state stress at the relative plate velocity. The rupture is initiated by stress unloading in a small region at about 7 km, and during the instability the stress in the whole rupture zone, the extent of which is defined by continuity of stress or zero stress intensity as mentioned in the previous section, is relaxed to the lower level associated with the high rupture speed (line A). Because of this stress

Slip

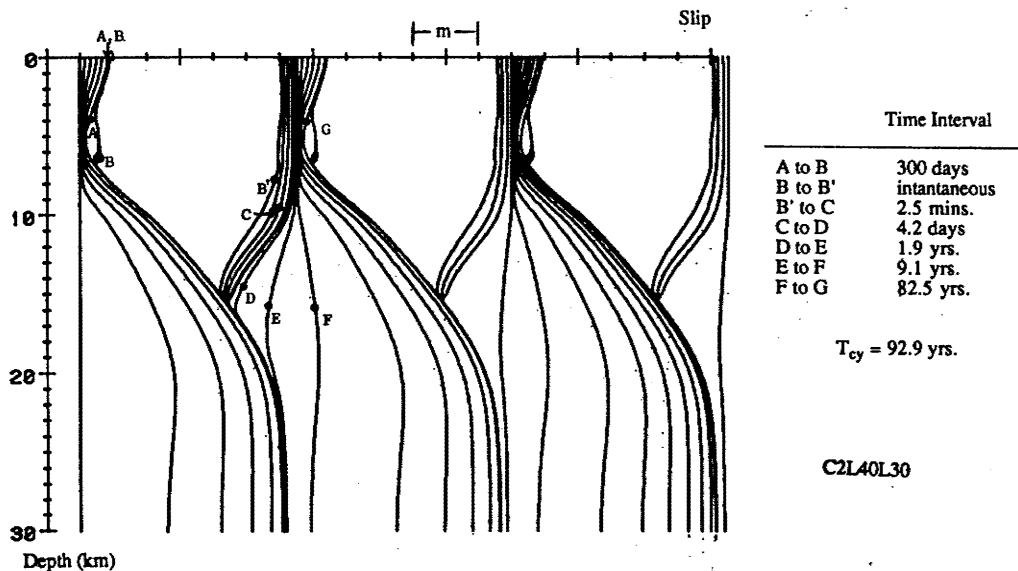| Time Interval	
A to B	300 days
B to B'	intantaneous
B' to C	2.5 mins.
C to D	4.2 days
D to E	1.9 yrs.
E to F	9.1 yrs.
F to G	82.5 yrs.

$T_{cy} = 92.9$ yrs.

C2L40L30

Fig. 10. Plots of depth distribution of slip at constant time. The simulation is identical to that of Figure 7 except that 30% dynamic overshoot in stress is included (C2L40L30).
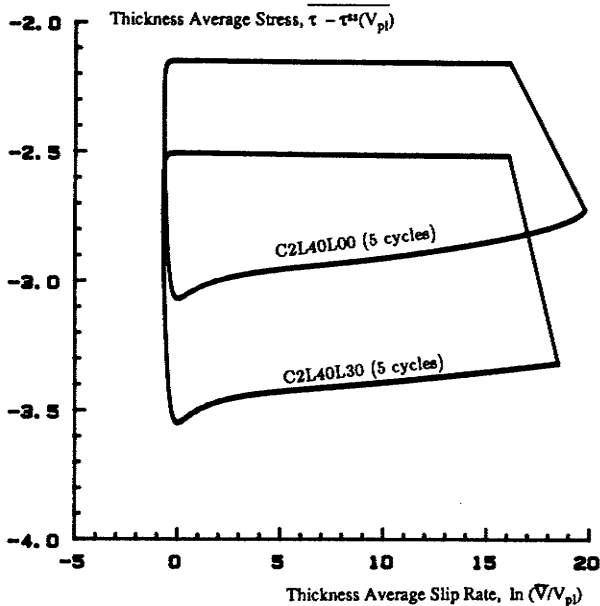
Fig. 11. Phase diagrams of the logarithm of the normalized thickness-averaged slip rate versus thickness-averaged differential stress for the case 2 with equation (5) as the steady state stress law and $L = 40$ mm.

unloading in the rupture zone the stress in the ductile zone below increases simultaneously. A short time after the earthquake (lines B to C), the stress in the rupture zone continues to decrease, and the stress in the ductile zone also continues to increase, causing the rapid postseismic creep.

Some parameters for the case presented in Figures 7–9 are listed in the first row of Table 1. Table 1 includes also, for easy comparison, parameters for a series of other simulations which we now discuss. Obviously, the details of the features described above would be altered by different assumptions regarding dynamic overshoot and steady state stress response. For instance, inclusion of dynamic overshoot in stress increases proportionally the coseismic slip and correspondingly reduces the postseismic slip in the rupture zone as shown in

Figure 10 (simulation C2L40L30) for the case identical to that in Figure 7 except that 30% dynamic overshoot in stress is included. However, this dynamic overshoot does not seem to increase much the overall cycle time, which is about 93 rather than 84 years. In order to show the periodicity of the earthquake cycle simulations, the logarithm of the normalized thickness-averaged slip rate versus the thickness-averaged differential stress is plotted in Figure 11 for the two simulations mentioned so far. It is clear in Figure 11 that the earthquakes repeat each other very closely. Similar situations arise when a different steady state stress law is chosen. Figure 12 (simulation C2L40N00) shows the plot of slip versus depth for the case identical to that in Figure 7 except that the steady state law is replaced by equation (3b); that is, the steady state stress is proportional to the logarithm of the normalized slip rate at all speeds. This means that a larger stress drop in the rupture zone is expected, and consequently, it takes a longer time (longer cycle time) to build up the stress for next earthquake instability. In comparison with Figure 7, Figure 12 has larger coseismic slip and smaller postseismic slip, while the amount of preseismic slip is about the same. Figure 13 (simulation C2L40N30) shows the plot of slip vs depth for the case identical to that in Figure 12 except that 30% dynamic overshoot in stress is included. Similarly, the coseismic slip is larger, but more significantly, the rupture zone begins to be arrested and effectively locked much earlier than the earlier case. This is mainly due to the large stress reduction from the preinstability stress state in the rupture zone.

From the standpoint of frictional sliding as modeled by our constitutive description, stress relaxation is accomplished by slip. This means that the amount of preseismic and postseismic slips is related to the magnitudes of the characteristic slip distance L. Larger preseismic and postseismic slips are consequences of larger L (or smaller $B - A$ in the shallow crust). Figure 14 (simulation C2L10L00) shows the plot of slip versus depth for the case identical to that in Figure 7 but the characteristic slip distance L is taken to be 10 mm, a factor of 4 smaller. As seen in Figure 14, both the preseismic and postseismic slips are less pronounced than those in Figure 7. Figure 15 (simulation C2L10L30) shows the plot of slip versus

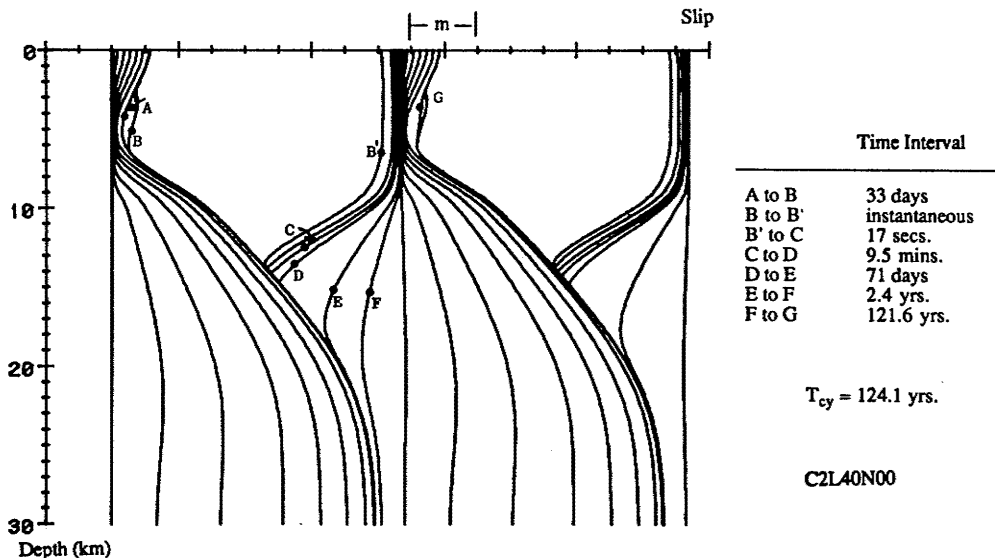| Time Interval	
A to B	33 days
B to B'	instantaneous
B' to C	17 secs.
C to D	9.5 mins.
D to E	71 days
E to F	2.4 yrs.
F to G	121.6 yrs.

$T_{cy} = 124.1$ yrs.

C2L40N00

Fig. 12. Plots of depth distribution of slip at constant time. The simulation is identical to that of Figure 7 except that the steady state stress law is proportional to ln (slip rate) at all speed (C2L40N00), so that there is a larger drop in stress for seismic slip.

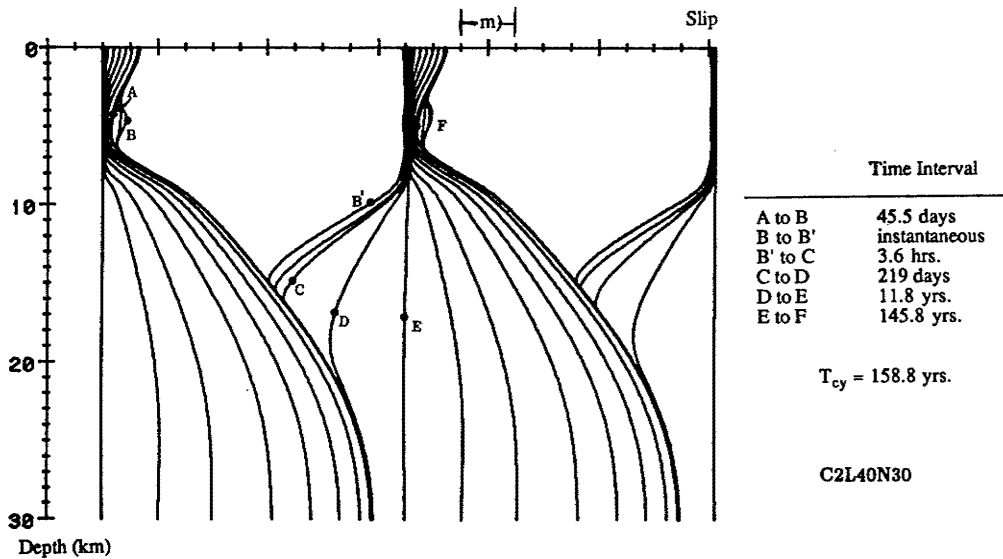| Time Interval	
A to B	45.5 days
B to B'	instantaneous
B' to C	3.6 hrs.
C to D	219 days
D to E	11.8 yrs.
E to F	145.8 yrs.

$T_{cy} = 158.8$ yrs.

C2L40N30

Fig. 13. Plots of depth distribution of slip at constant time. The simulation is identical to that of Figure 12 except that 30% dynamic overshoot in stress is included (C2L40N30).

depth for the case identical to that in Figure 14 except that 30% dynamic overshoot in stress is included. Because of the dynamic overshoot, there is yet less postseismic slip.

Two more simulations are included to show the effect of the magnitude of $B - A$ in the shallow crust on the presesimic and postseismic slips. Figures 16 (C1L40L00) and 17 (C1L40L30) are identical to the cases shown in Figures 7 and 10, respectively except that a smaller (about half) magnitude of $B - A$ in the shallow crust is used (i.e., case 1 of Figures 1 and 3). This corresponds to a situation in which the shallow fault material behaves in a less brittle manner. As seen in both Figures 16 and 17, larger preseismic and postsesimic slips are observed as compared to Figures 7 and 10. Now the nucleation depths (again, around 7 km) are stressed not only by slip below but also by short-term preseismic slip above. In addition, since the material is less brittle, there is less stress drop, hence less coseismic slip and a shorter earthquake cycle.

The differences in the above eight simulations discussed so far are summarized in Table 1. We have not mentioned cases for which $A - B$ is positive even at shallow depths. These would lead to steady sliding at V_{pl} at all depths and no earthquakes.

The order of magnitude of the predicted cycle time and the difference in cycle time with different steady state stress laws can be estimated in the following way. It is reasonable to expect that the majority of the cycle time is spent stressing the seismogenic zone when it is effectively locked. The time it takes to increase the stress in the zone and then break the zone is equal to $\Delta\tau/\dot\tau$, where $\Delta\tau$ and $\dot\tau$ are the stress increase and the stressing rate, respectively. The stressing rate must be estimated in a manner which includes the nearly steadily slipping ductile flow region below. Using crack mechanics solutions [Tse et al., 1985; Tse, 1985], one can easily estimate this stressing rate in the locked region. Without going through the

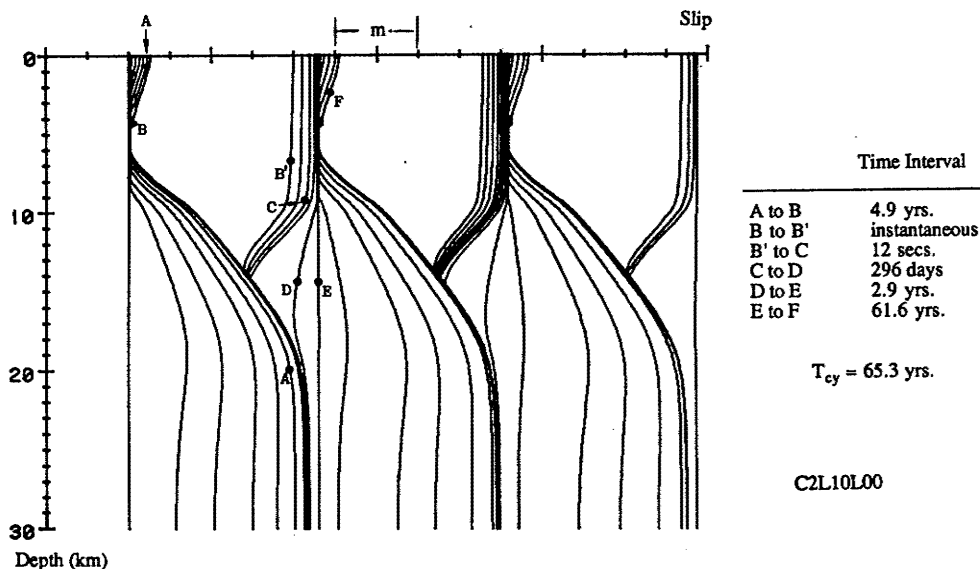| Time Interval	
A to B	4.9 yrs.
B to B'	instantaneous
B' to C	12 secs.
C to D	296 days
D to E	2.9 yrs.
E to F	61.6 yrs.

$T_{cy} = 65.3$ yrs.

C2L10L00

Fig. 14. Plots of depth distribution of slip at constant time. The simulation is identical to that of Figure 7 except that the characteristic slip distance L is taken to be 10 mm (C2L10L00).

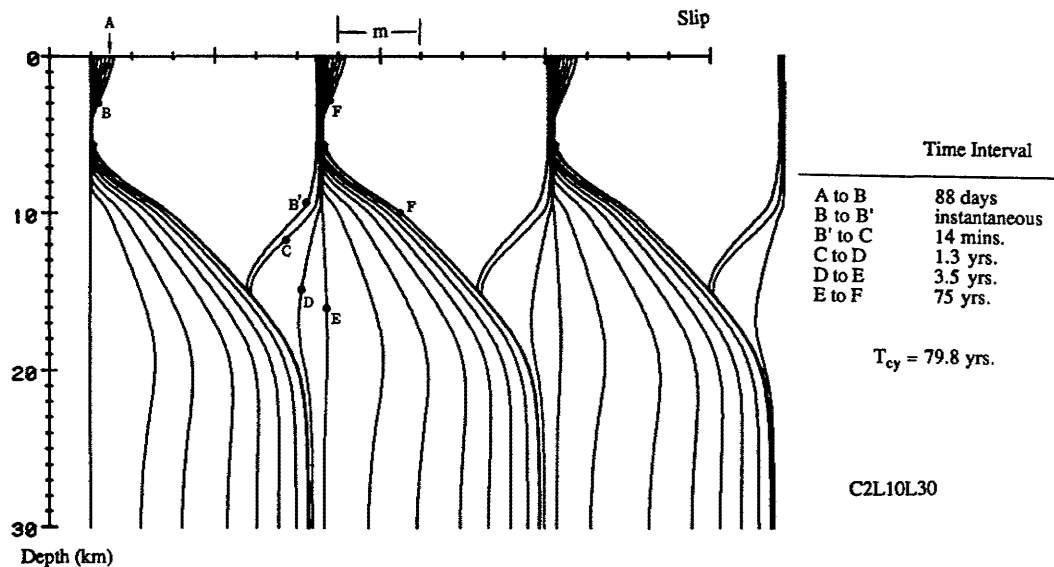| Time Interval	
A to B	88 days
B to B'	instantaneous
B' to C	14 mins.
C to D	1.3 yrs.
D to E	3.5 yrs.
E to F	75 yrs.

$T_{cy} = 79.8$ yrs.

C2L10L30

Fig. 15.   Plots of depth distribution of slip at constant time. The simulation is identical to that of Figure 14 except that 30% dynamic overshoot in stress is included (C2L10L30).

mathematical details here, we estimate that the stressing rate $\dot{\tau}$ in the middle of a locked patch is about 0.06 MPa/yr. On the other hand, one can also relate the stress increase $\Delta\tau$ to the stress drop associated with the instability; i.e., $\Delta\tau = \tau^{(1)} - \tau^{ss}(V_L)$. Roughly, $\tau^{(1)}$ can be identified with $\tau^{ss}(V_{pl})$. One can see that the steady state stress law (5) would give rise to a lower stress increase than the one using the steady state stress law (3b). For case 2 and neglect of dynamic overshoot in stress, $\Delta\tau$ is about 3.5 MPa for the law (5) and 6.5 Mpa for the law (3b). Hence the times spent in the effectively locked stage are about 60 years and 109 years, respectively. The simulations have predicted the time in the locked stage as 84 years for the law (5) and 124 years for the law (3b). However, this simple estimation of cycle time assumes no stress relaxation (i.e., no slip in the effectively locked zone); any stress relaxation would reduce the stressing rate to the effectively locked region and thus would increase the cycle time. This can be seen from Table 1, where the cycle times with $L = 40$ mm are

longer than those with $L = 10$ mm (compare rows 1 and 5, 2 and 6). We can, of course, estimate the total slip by multiplying the cycle time by the relative plate velocity. It is interesting to see that the cycle time in a variable slip system depends on the accentuation of the stressing rate due to the deeper slip.

Except for the characteristic slip distance L the parameters used in the present simulations are constrained by the relative plate velocity, San Andreas fault geotherm, and the presently incomplete experimental data from friction tests (e.g., A and B). While our simple extrapolations for the depth variations of A and B are questionable, we have shown that the cycle time depends on the stress change $\Delta\tau$ discussed above and this increases with the magnitude of $A - B$ through the steady state stress law (3b) or (5). Hence one can expect that more negative $A - B$ would give a longer cycle time, which is the situation for the cycle times predicted from cases 1 and 2 (compare rows 1 and 7, 2 and 8 in Table 1). This consequently

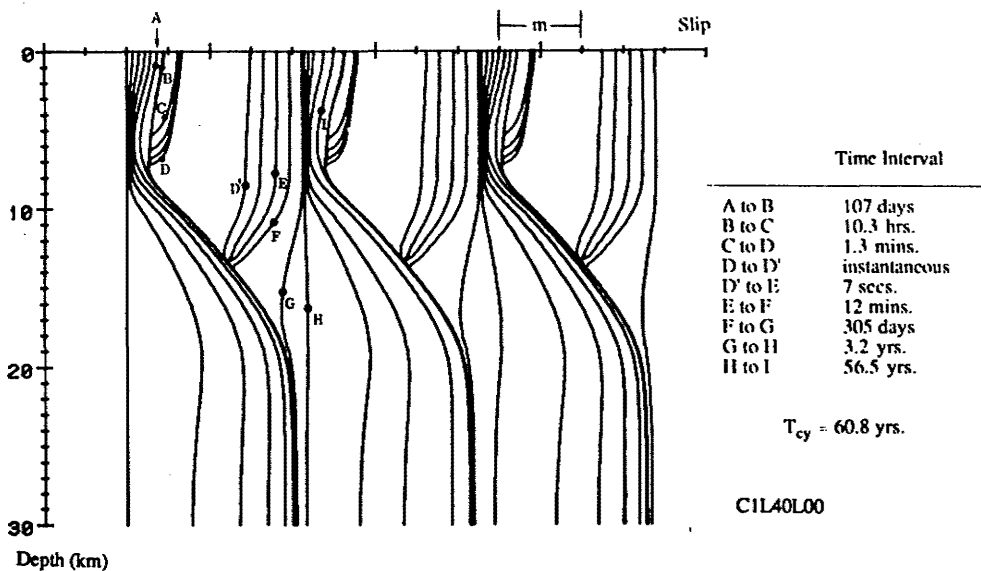| Time Interval	
A to B	107 days
B to C	10.3 hrs.
C to D	1.3 mins.
D to D'	instantaneous
D' to E	7 secs.
E to F	12 mins.
F to G	305 days
G to H	3.2 yrs.
H to I	56.5 yrs.

$T_{cy} = 60.8$ yrs.

C1L40L00

Fig. 16.   Plots of depth distribution of slip at constant time. The simulation is identical to that of Figure 7 except that the depth distributions of A and B are denoted by case 1 in Figures 1 and 3 (C1L40L00).

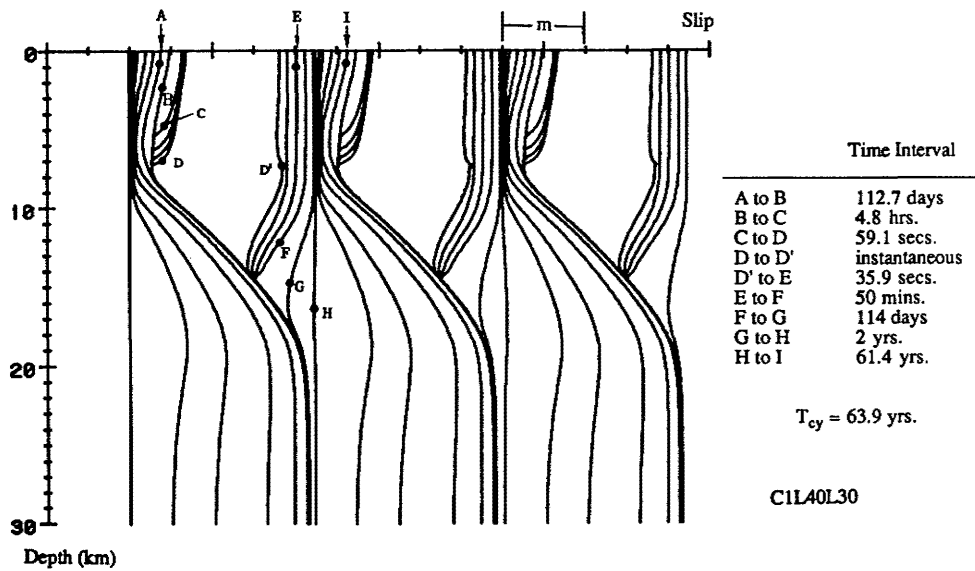| A to B	112.7 days
B to C	4.8 hrs.
C to D	59.1 secs.
D to D'	instantaneous
D' to E	35.9 secs.
E to F	50 mins.
F to G	114 days
G to H	2 yrs.
H to I	61.4 yrs.

$T_{cy} = 63.9$ yrs.

C1L40L30

Fig. 17. Plots of depth distribution of slip at constant time. The simulation is identical to that of Figure 16 except that 30% dynamic overshoot in stress is included (C1L40L30).

leads to larger total slip and seismic slip. More generally, for the same geological setting, different faulting behavior can be simulated by different types of frictional response (i.e., different types of A and B variations if we use the class of friction law presented here). For instance, the creeping section of the San Andreas fault in central California can be simulated by an $A - B$ distribution that is positive (velocity strengthening) over even the shallow depth range.

Finally, it should be mentioned that in the present simulations we take the characteristic slip distance L to be 10 and 40 mm, values which are 2-3 orders of magnitude higher than laboratory-determined values but which may possibly be more appropriate in terms of scaling of fault irregularities to the crustal scale. Simulations involving smaller values of L are costly. In order to help toward a comprehensive insight into effects that L has upon the simulations, we have done simulations over a wide range of L for case 2 of Figures 1 and 3, with the steady state stress law (5); that is, steady state stress becomes independent of slip rate at speed above 0.1 mm/s. As mentioned before, for L above 160 mm, the system is stable and slips steadily at V_{pl} at all depths. For L between about 80 mm and 160 mm the system is in a transitional stage in the

sense that instead of earthquake instability with sudden slip, the velocity weakening crustal zone catches up with the ductile zone below by stable but fast episodic creep events. For L below 80 mm, earthquake instability always results. The cycle time, rupture initiation depth, rupture extent, and total and coseismic slips are summarized in Table 2.

In order to numerically simulate the onset of an earthquake instability sensibly in a continuous medium, one obviously should require that results be independent of grid element size in the numerical discretization. We find that a good indication that the grid is too coarse is that a single grid point accelerates to limiting seismic speed and unloads before its neighbors begin to react. Conversely, we find that grid size independence is sensibly achieved when we require that at least two neighboring grid points reach or exceed a limiting speed $V_L (=0.88$ m/s) at the same time. Hence since the size of the local unloading zone which leads to rupture nucleation decreases with the

TABLE 2. Summary of Earthquake Cycle Parameters for Simulations With Different Values of the State Relaxation Slip L

L, mm	Surface Slip, m		Depth, km		Cycle Time, years
	Total	Coseismic†	Initiation	Rupture Extent	
80	3.37	1.42	6.3	13.8	96
60	3.16	1.59	4.6	13.8	90
40	2.95	1.90	6.7	13.9	84
30	2.80	1.88	6.2	13.9	80
20	2.62	1.84	5.5	13.9	75
10	2.29	1.74	4.6	13.8	65
5	1.86	1.56	7.9	13.6	53

All are based on case 2 in Figures 1 and 3, on the steady state stress becoming independent of slip rate at speed above 0.1 mm/s, that is, equation (5) and on no dynamic overshoot of stress drop.

†See explanation in Table 1.

TABLE 3. Summary for the Cases Described in Table 2, Showing the Grid Sizes and Number of Grid Elements Over a Plate Thickness of 30 km, and the Rupture Initiation Zone Size Depending on the Choice of the Velocity Range

L, mm	Grid Size, m	Number of Elements	Rupture Initiation Zone Width, m	
			$0.11 < V$ < 0.88 m/s	$0.59 < V$ < 0.88 m/s
160	234	129	system completely stable	
80	234	129	1400	...
60	234	129	2600	468
	117	257	2200	468
40	117	257	700	*
	58.6	513	820	176
	29	1025	760	176
30	58.6	513	530	117
	29	1025	586	132
20	58.6	513	117	*
	29	1025	293	88
	14.6	2049	322	88
10	14.6	2049	234	44
5	7.3	4097	73	14.6

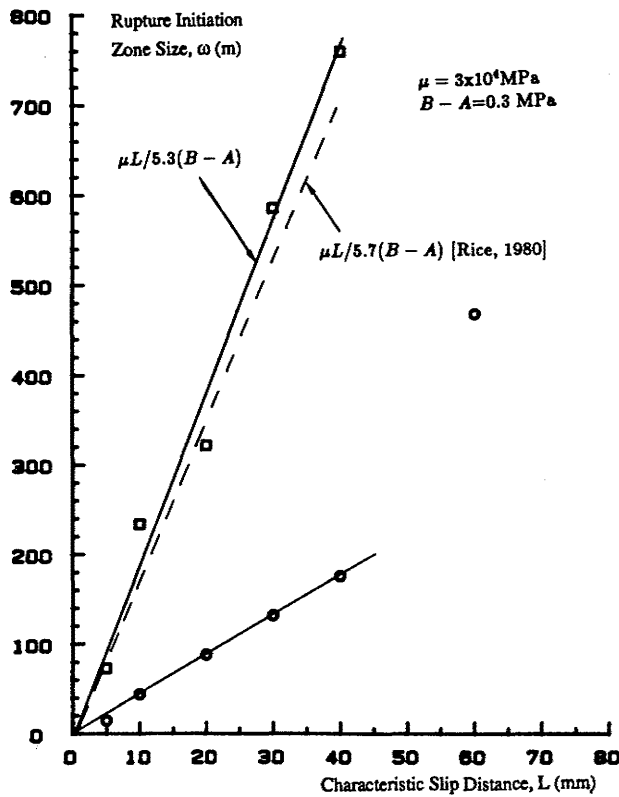*Only one grid element reaches limiting speed, 0.88 m/s.

Fig. 18. Plot of the characteristic slip distance L versus the rupture initiation zone size. Circles are for the rupture initiation zone over which the slip rate is between 0.59 m/s and $V_L = 0.88$ m/s. Squares are for the rupture initiation zone over which the slip rate is betwen 0.11 m/s and 0.88 m/s. The dashed line is from $\omega = \mu L/5.7(B - A)$ for the strength degradation zone size for a slip weakening crack in a linear elastic medium [Rice, 1980].

equation (5), then $\omega \simeq \mu L/5.7(B - A)$. Though arbitrary, a reasonable definition for the rupture initiation zone size, such as that in which the material points slide between 0.11 m/s and 0.88 m/s, yields an estimate of the proportionality constant which is reasonably close to the strength degradation zone size ω (Figure 18).

Last, the cycle time normalized by some characteristic cycle time T_1 (estimated from $\Delta\tau/\dot{\tau}$, as discussed above) is plotted against the characteristic slip distance L normalized by the seismogenic depth D in Figure 19. $D = 10$ km and $T_1 = 60$ years are used to prepare the Figure 19. The results are not of a form that one can confidently extrapolate for L in the range determined by laboratory studies (i.e., of the order of tens of microns).

Unfortunately, the calculations with the small grid size and hence many degrees of freedom necessary when $L = 5$ mm (Table 3) required computer time on the Cray I of approximately 3/4 hour per earthquake cycle. Since it is necessary to carry the calculations through several cycles to converge on the limit cycle which is then repeated periodically, the total time used for the $L = 5$ mm run was about 4 hours. Computer time more than doubles for each halving of L in the small L range. Thus even with quite large allotments of supercomputer time (approximately 25 hours on the Cray I was consumed for the various simulations summarized here in Tables 1, 2, and 3, for which more details are reported by *Tse* [1985] but not presented here; approximately 5 Cray I hours were spent initially developing and testing solution algorithms), it is not practial to do crustal scale earthquake cycle simulations of the type we report here with values of L much less than 5 mm. Also, for the particular structure of our program, the $L = 5$ mm case came close to saturating the available Cray I storage space. This is an unfortunate situation since a truely compre-
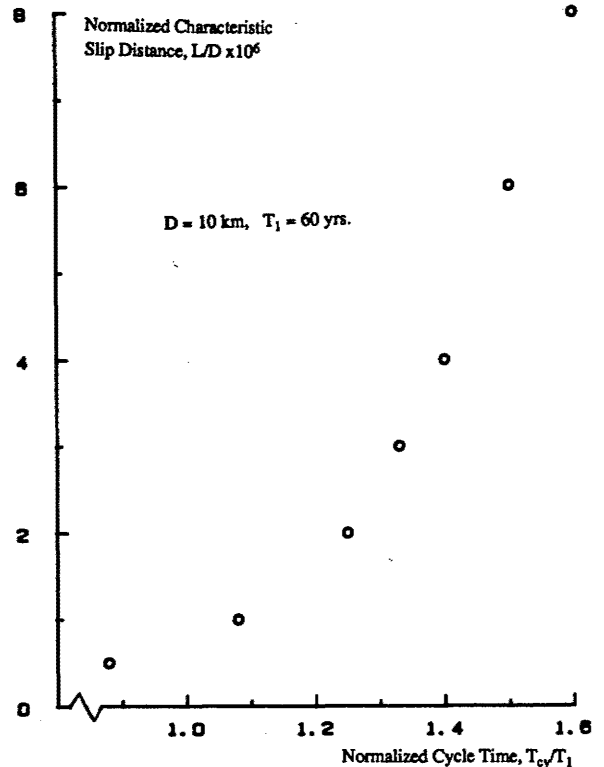
characteristic slip distance L, a correspondingly small grid size (and large number of differential equations of the form in equations (11) and (12) to be solved simultaneously) is required for a sensible numerical solution with small L. Presently, we are able to have simulations for L as low as 5 mm, and the grid size for this value of L is about 7 m. The grid sizes or the number of grid elements used in the simulations and the sizes of the zones in which the material points slide at speeds between 0.11 m/s and 0.88 m/s and between 0.59 m/s and 0.88 m/s are summarized in Table 3. The sizes of these zones are also plotted agaist the characteristic slip distance L, as shown in Figure 18. It seems that within some modest variation the size of rupture initiation zone increases linearly with L for small L. At large L the rupture initiation zone size deviates away from the linear variation to larger values. This reflects the situation that for large L the system becomes more stable and involves essentially the whole seismogenic layer. On the other hand, the linearity of the rupture initiation zone size with the characteristic slip distance L in the range of small L can be seen from the following. For a mode III crack in an infinite linear elastic medium with the crack face subjected to friction stress which decreases gradually from a static friction stress at zero slip to a lower constant friction stress in slip over a characteristic slip weakening distance L, *Rice* [1980] estimated that the size of the strength degradation zone ω (cohesive zone near the crack tip) is proportional to the slip weakening distance L and is given by $\omega = 9\pi\mu L/16\Delta\tau$. If one estimates the stress drop $\Delta\tau$ by $\Delta\tau = \tau^{ss}(V_{pl}) - \tau^{ss}(V_L)$ from

Fig. 19. Plot of the normalized cycle time versus the normalized characteristic slip distance.

hensive understanding of the effect of L, extending to L values in the 1-mm range and below, cannot be attained. One expects, for example, that the limit of solutions of the type we discuss here as $L \to 0^+$ is not meaningful, since that limit would seem to involve the same sort of defects and paradoxical situations associated with using classical friction concepts (without finite slip weakening distances), developed for systems of interconnected rigid blocks, in continuum models.

Study of the rupture initiation depths in Table 1 and 2 shows that this parameter varies in an unpredictable manner from one simulation to another, even when the different simulations cause only small changes in other parameters. There is a tendency for nucleation to occur in the general vicinity of the maximum of $B - A$ (i.e., near the most "brittle" depth in the crust). This maximum occurs at 6.5 km depth for case 2, assumed for all entries of Table 2 and all of Table 1 except the last two, which are case 1. The depth of maximum $B - A$ is 8.5 km for case 1. Possibly, the initiation depth is highly sensitive to details of the distribution of $A - B$ in the brittle zone. If so, the depth must be regarded as essentially unpredictable since the data summarized in Figure 1 clearly do not allow reliable detailed modeling of property variations with depth. Part of the unpredictability follows from the fact that in most of our simulations (e.g., for all shown here except that of Figure 13 and possibly Figures 16 and 17), initiation occurs either near the top or the bottom of the most locked section of the shallow crust, where slip above and below concentrates stress onto that section. Evidently, with minor changes in the detailed depth variations, the rupture initiation depth can be shifted from the top to the bottom or vice versa. For the exception noted in Figure 13, initiation occurs toward the middle of the most locked zone, whereas in Figures 16 and 17 it occurs toward the bottom but seems to be triggered by a creep event that spreads down from the top. If the very shallow (0–3 km) portion of the crust does not actually slip and concentrate stress at the top of a locked zone or if the very shallow crustal deformation actually occurs as distributed rather than single-fault localized strain, then we would expect initiation to generally (rather than just sometimes, as in our simulations) occur at the bottom of the locked zone where stress is concentrated from slip below. The latter is the rupture initiation mechanism suggested in previous studies involving the cracklike penetration of slip into a previously locked zone [*Dmowska and Li*, 1982; *Li and Rice*, 1983; *Tse et al.*, 1985].

SUMMARY DISCUSSION:
ASSUMPTIONS, CONCLUSIONS, AND OBSERVATIONS

Our modeling of the great strike-slip earthquake cycle is based on the following three primary assumptions:

1. Inelastic crustal deformation during the earthquake cycle can be idealized as being localized to a fault surface which penetrates deeply into the lithosphere or at least penetrates significantly below the depth of the seismogenic zone.

2. The constitutive relations between stress and slip on that fault have the same general structure as revealed in laboratory fault slip (friction) studies. By this we mean that the fault surface has an inherently positive instantaneous rate sensitivity and that the stress τ evolves with ongoing slip toward a steady state strength $\tau^{ss}(V)$, which is a function of the current slip velocity V. We further assume that the evolution of the stress can be adequately represented by the class of constitutive relations given by equation (2).

3. Laboratory friction data on Westerly granite, as a rep-

resentative rock type of the continental crust, can be used to infer approximately the velocity, temperature, and effective normal stress dependence of the instantaneous rate sensitivity $A[=(\partial\tau/\partial \ln V)_{inst.}]$ and long-term rate sensitivity $A - B[= d\tau^{ss}(V)/d \ln V]$. By contrast, however, the state evolution slip distance L is regarded, compatibly with other attempts to extend laboratory fracture mechanics concepts to the crust, as a parameter which scales to values larger than those of laboratory studies owing to larger geometric irregularities at the crustal scale.

The experimental data base on which one could translate assumption (3) into a depth variation of constitutive quantities for the crust is incomplete. The important temperature range above room temperature but below 300°C is without appropriate data. Also, there is lack of systematic study of normal stress dependence of the rate sensitivity. Nevertheless, by assuming temperature independence at low temperature, we can fit the existing data for A and $A - B$ as a function of temperature as in Figure 1 and assume proportionality to normal stress except at very high temperatures. This leads to the depth variations of frictional slip properties as shown in Figure 3. A critical feature of these variations is the transition, at about 11 km based on a San Andreas fault geotherm, from velocity weakening ($A - B < 0$) in the shallow crust to velocity strengthening ($A - B > 0$) at greater depths. The velocity independence of A and $A - B$ at low V is supported by laboratory data, but the data range extends downward only to around 0.1 μm/s. We extrapolate this down to the tectonic plate velocity and below as in Figure 4, continuing the linear variation with $\ln V$. Also, in different quasi-static simulations of the detailed mechanics of the resulting earthquake cycle for a large-scale crustal model, Figure 5, we explore the options of leveling-off $\tau^{ss}(V)$ at larger V (Figure 4) and accounting for a dynamic overshoot in the stress drop associated with each great earthquake. The mechanics analysis ignores variations along strike and neglects asthenosphere resistance, but the fault zone is loaded in a manner consistent with accommodation of a uniform average plate velocity of 35 mm/yr, appropriate for the San Andreas fault.

Among significant observations and conclusions from our work we mention the following:

1. The transition in the character of fault frictional response from velocity weakening at shallow, cooler depths to strengthening at greater, hotter depths, as is clearly suggested by the laboratory data, is of itself sufficient to explain the observed shallow depth confinement of crustal seismicity. This is a definitive conclusion, anticipated from known associations between velocity strengthening and stability and clearly confirmed in our detailed numerical simulations (Figures 7–17). In particular, it is seen that the shallow depth confinement of seismicity does not require for its explanation that there be a transition at the base of the seismogenic layer from a zone of fault-localized deformation to a zone of broadly distributed creep flow. The latter transition may in fact occur, but arguments in its favor, as opposed to the deep fault model studied here, should be based on data other than the depth confinement of seismicity. With either conception of deformation style in the deeper crust, seismicity is depth confined because the prevailing stresses are relaxed substantially below the levels required for rapid slip; see Figure 4b and associated discussion for the present deep fault model.

2. The simulations resulted in periodic limit cycles that model recurring earthquakes or, at larger L, episodic stable

creep events; at very large L the fault surface slides at a uniform rate equal to the plate velocity. The nature of the constitutive response is such that regain of resistance to slip gradually occurs in the slow creep slippage process following the last instability. The limit cycles appear to be unique, for a given depth variation of constitutive properties, but it is not known whether, for example, starting the calculations with dramatically different initial conditions could lead to different limit cycles or perhaps to aperiodic cycles; neither case was encountered in our work.

3. The predicted earthquake cycles involve overall features which appear to be in good agreement with the accepted phenomenology of strike-slip earthquakes along the San Andreas fault. These overall features seem to require for their prediction only the existence of a transition from velocity stengthening to velocity weakening along lines at least somewhat like what we infer in Figures 1–4 based on existing data. Although more detailed features of the predicted earthquake cycles are of course dependent on details of the depth variation assumed for constitutive properties and on other aspects of the modeling procedure (e.g., inclusion of dynamic overshoot), it is significant to recognize that no ad hoc or specialized assumptions were necessary to achieve the overall agreement (unless we consider the use of L values larger than laboratory size to be ad hoc). The overall features referred to are well documented in Figures 7–17. They include the development of an effectively locked patch (region with V much smaller than V_{pl}) in the velocity weakening part of the crust above about 11 km within less than a year after the last great earthquake, while the velocity strengthening portion of fault surface below 11 km slips continually at a speed of the order of, but less than, V_{pl} through most of the cycle. As the cycle goes on, the slipping zone gradually penetrates upward into the locked zone (as found also in previous slip weakening and crack modeling) so that the affected portions of the velocity weakening zone are then caused to slip more or less steadily at a fraction of V_{pl}. This is evident in all our figures showing slip versus depth. Finally, a small portion of the effectively locked zone begins to unload with accelerating slip, and this rapidly spreads and becomes the earthquake instability. The coseismic motions are relatively uniform over the effectively locked zone, reduce slightly in magnitude near the earth's surface (where some aseismic slip through much of the cycle is inevitably predicted), and taper off gradually to zero at 13–15 km depth. The zone moving coseismically thus includes a depth range with velocity strengthening which had slipped at a healthy fraction of V_{pl} throughout most of the cycle. Rapid postseismic slip continues over another 3–4 km depth below the seismic rupture zone, but V there has reduced to a value close to V_{pl} after a few years. Earthquake cycle time for the broad range of parameters which we have examined (Tables 1 and 2) ranges from about 50 to 160 years.

4. The initiation depth for the seismic rupture varies from about 3 to 8 km in our simulations and seems to change unpredictably with small changes in the constitutive description. Close examination reveals that this initiation site generally (but not always) lies at either the lower or upper border of the effectively locked zone. As commented in item 3, slip is predicted to penetrate into the effectively locked zone from below. It does so also from above, owing to relaxation in the very shallow crust. Sometimes the disturbance from above nucleates the instability first and sometimes that from below. As mentioned in the text, a modification of the very shallow crustal properties which made initiation from above less likely would then seem to favor initiation at the base of the effectively locked zone, as the general rule, and such would seem to agree better with seismic inferences of 7–10 km depth as representative initiation depths.

5. We present an evaluation of the effect of the size of L over a wide range and show that the size of the grid elements in a numerical discretization must scale approximately with L, at small L, for an accurate solution to be obtained. This unfortunately makes for prohibitively time-consuming computations for L much below 5 mm (the smallest that we examine), even with access to present-day supercomputers.

6. Every result that we present from the simulations is dependent only on the changes of τ with V (and previous V history) at each depth along the fault. The results have no dependence whatever on the absolute level of τ for a given V history or on the variation of that absolute level with depth. These latter features would be important if we were to check (as we do not) whether the assumed temperature variation with depth is compatible with heating from our predicted fault slip histories. However, the former features (i.e., how τ changes with V and its history) are critical to understanding whether fault slip is stable or unstable and to determining all aspects of the earthquake cycle. Their importance often goes unrecognized, e.g., in discussion of frictional strength of the crust which focus only on an absolute strength level for frictional sliding and not on the character of that sliding.

7. Our simulations do not incorporate any features which could explain seismic events of various magnitudes (e.g., described by a frequency-magnitude relation), in addition to the great earthquake, during a cycle. Nor do they explain foreshocks of the major event (at least not in a respectable way; use of an inadequately large grid size, compared to that needed for correct simulation of the continuum model, can lead to confined instability events before the major rupture). Thus in the present simulations we can interpret such lower level seismicity only as noise associated with what appears to be stable slipping at the megascopic scale, perhaps analogous to laboratory acoustic emission during a stable frictional slip experiment. For similar reasons our modeling concepts seem inadequate to deal with the local scale heterogeneity of faulting, often described in terms of "asperities" and "barriers" and leading to inferred local stress drops which can be much larger than the values in our simulations, which correspond more to average stress drops over large rupture areas. Possibly, future full-cycle instability modeling could address the heterogeneity issue by assumption of some combination of random variation in constitutive parameters and complex nonplanar segmentation of the fault.

APPENDIX

In this section, two-dimensional linear elastic theory is used to derive a solution for a line screw dislocation of magnitude δ at $y = 0$, $z = a$ in an infinite plate of thickness H as shown in Figure A1a. The only nonvanishing displacement is $u(y, z)$ in the x direction. With the stress-strain and strain-displacement relations, one can rewrite the stress equilibrium equation as $\nabla^2 u = 0$ for this case where ∇^2 is the Laplacian operator in the y-z plane. Displacement and shear stresses may then be represented in terms of an analytic function $\omega(z + iy)$ of the complex variable $z + iy$:
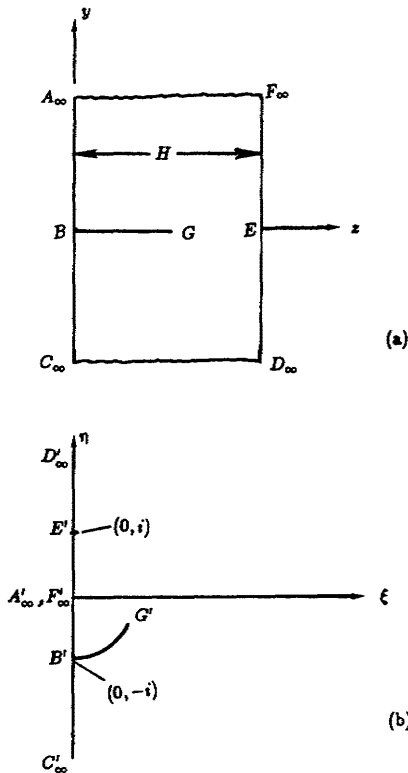
$$u = \text{Im } [\omega(z + iy)] \qquad (A1)$$

Fig. A1. (a) An infinite strip of width H with a screw dislocation at G. $z = 0$ and $z = H$ are stress free. (b) Conformal mapping of the strip in Figure A1a onto a half plane. The screw dislocation is at G' and $\zeta = 0$ is the stress free boundary.

and

$$\tau_{xy} + i\tau_{xz} = \mu\omega'(z + iy) \qquad (A2)$$

where μ is the shear modulus.

The aim of this analysis is to find the analytic function meeting the appropriate boundary conditions. In particular, the top ($z = 0$) and the bottom ($z = H$) faces of the plate are stress free. That is, along $A_\infty BC_\infty$ and $D_\infty EF_\infty$, $\partial u/\partial n = 0$, where n is the measured normal to the faces concerned. The displacement jump across the dislocation line BG is $u(y = 0^+, z) - u(y = 0^-, z) = \delta$. The analytic function $\omega(z + iy)$ may be found readily if one first conformally maps the strip in Figure A1a into a right half plane (Figure A1b) with a mapping function $\zeta + i\eta = -i \exp[i\pi(z + iy)/H]$. In this mapped half plane the imaginary axis corresponds the stress free boundary, while $B'G'$ corresponds to the line over which the displacement jump is δ. Knowing the screw dislocation solution in an infinite plane is of the form of $\ln(\zeta + i\eta - \rho)$, where ρ is the (complex) location of the dislocation line, the solution in a half plane as shown can be generated by superposition of two screw dislocations in an infinite plane with one at ρ and the other of opposite magnitude at a point which is the mirror image of ρ with respect to the imaginary axis. Therefore the analytic function $\omega(z + iy)$ for this problem is given by

$$\omega(z + iy) = A \ln\left[\frac{\zeta + i\eta + ie^{i\pi a/H}}{\zeta + i\eta + ie^{-i\pi a/H}}\right] \qquad (A3a)$$

or

$$u(y, z) = A \operatorname{Im}\left[\ln\left(\frac{e^{i\pi(z+iy)/H} - e^{i\pi a/H}}{e^{i\pi(z+iy)/H} - e^{-i\pi a/H}}\right)\right] \qquad (A3b)$$

where A is a constant to be found from matching the displacement jump $\delta = u(0^+, z) - u(0^-, z)$ across BG. Thus, with (A3b),

$$A = -\frac{\delta}{2\pi} \qquad (A4)$$

and the stresses are calculated from (A2) as

$$\tau_{xy} + i\tau_{xz} = -\frac{\mu\delta}{4H}\left[\frac{\sin\dfrac{\pi a}{H}}{\sin\dfrac{\pi(z + iy - a)}{2H}\sin\dfrac{\pi(z + iy + a)}{2H}}\right] \qquad (A5)$$

On the earth's surface ($z = 0$) the shear strains are

$$\gamma_{xy} + i\gamma_{xz} = -\frac{\delta}{4H}\left[\frac{\sin\dfrac{\pi a}{H}}{\sin\dfrac{\pi(iy - a)}{2H}\sin\dfrac{\pi(iy + a)}{2H}}\right]$$

$$= -\frac{\delta}{2H}\left[\frac{\sin\dfrac{\pi a}{H}}{\cos\dfrac{\pi a}{H} - \cosh\dfrac{\pi y}{H}}\right] \qquad (A6)$$

Along the slip boundary, $y = 0$, one can find the Green's function $G(z, a)$ as defined in (7a) as

$$G(z, a) = \frac{\mu}{4H}\left[\frac{\sin\dfrac{\pi a}{H}}{\sin\dfrac{\pi(z - a)}{2H}\sin\dfrac{\pi(z + a)}{2H}}\right] \qquad (A7)$$

REFERENCES

Brace, W. F., and J. D. Byerlee, Stick-slip as a mechanism for earthquakes, *Science, 153,* 990–992, 1966.

Burridge, R., and G. S. Halliday, Dynamic shear cracks with friction as models for shallow focus earthquakes, *Geophys. J. R. Astron. Soc., 25,* 261–283, 1971.

Chen, W. P., and P. Molnar, Focal depths of intracontinental and intraplate earthquakes and their implications for the thermal and mechanical properties of the lithosphere, *J. Geophys. Res., 88,* 4183–4214, 1983.

Dieterich, J. H., Earthquake mechanisms and modeling, *Annu. Rev. Earth Planet. Sci., 2,* 275–301, 1974.

Dieterich, J. H., Time-dependent friction and the mechanics of stick-slip, *Pure Appl. Geophys., 116,* 790–806, 1978.

Dieterich, J. H., Modeling of rock friction, 1, Experimental results and constitutive equations, *J. Geophys. Res., 84,* 2161–2168, 1979a.

Dieterich, J. H., Modeling of rock friction, 2, Simulation of preseismic slip, *J. Geophys. Res., 84,* 2169–2175, 1979b.

Dieterich, J. H., Experimental and model study of fault constitutive properties, in *Solid Earth Geophysics and Geotechnology, AMD Symp. Ser.,* vol. 42, edited by S. Nemat-Naser, pp. 21–29, American Society of Mechanical Engineers, New York, 1980.

Dieterich, J. H., Constitutive properties of faults with simulated gouge, in *Mechanical Behavior of Crystal Rocks, Geophys. Monogr.*

Ser., vol. 24, edited by N. L. Carter, M. Friedman, J. M. Logan, and D. W. Stearns, pp. 103–120, AGU, Washington D. C., 1981.

Dieterich, J. H., and G. Conrad, Effect of humidity of time- and velocity-dependent friction in rocks, J. Geophys. Res., 89, 4196–4202, 1984.

Dmowska, R., and V. C. Li, A mechanical model of precursory source processes for some large earthquakes, Geophys. Res. Lett., 9, 393–396, 1982.

Eaton, J. P., M. E. O'Neill and J. N. Murdock, Aftershocks of the 1966 Parkfield-Cholame, California, earthquake: A detailed study, Bull. Seismol. Soc. Am., 60, 1151–1197, 1970.

Gu, J.-C., J. R. Rice, A. L. Ruina, and S. T. Tse, Slip motion and stability of a single degree of freedom elastic system with rate and state dependent friction, J. Mech. Phys. Solids, 32, 167–196, 1984.

Hill, D. P., P. Mowinckel, and K. M. Lahr, Catalog of earthquakes in the Imperial Valley, California, June 1973–May 1974, U.S. Geol. Surv. Open File Rep., 25-041, 29 pp., 1975.

Lachenbruch, A. H., and J. H. Sass, Thermo-mechanical aspects of the San Andreas, Proceedings, Conference on the Tectonic Problems of the San Andreas Fault System, edited by R. L. Kovach and A. Nur, Stanford Univ. Publ. Geol. Sci., 13, 192–205, 1973.

Li, V. C., and J. R. Rice, Preseismic rupture progression and great earthquake instabilities at plate boundaries, J. Geophys. Res., 88, 4231–4246, 1983.

Mavko, G. M., Simulation of earthquakes and creep events on a spatially variable model (abstract), Eos Trans. AGU, 61, 1120, 1980.

McHugh, C. A., and F. W. Lester, Catalog of earthquakes along the San Andreas fault system in central California for the year 1976, U.S. Geol. Surv. Open File Rep., 78-1051, 99 pp., 1978.

Meissner, R., and J. Strehlau, Limits of stresses in continental crust and their relationship to the depth-frequency distribution of shallow earthquakes, Tectonics, 1, 73–79, 1982.

Rice, J. R., The mechanics of earthquake rupture, in Physics of the Earth's Interior, Proc. Int. Sch. Phys. "Enrico Fermi," 78, edited by A. M. Dziewonski and E. Boschi, pp. 555–649, North Holland, Amsterdam, 1980.

Rice, J. R., Constitutive relations for fault slip and earthquake instabilities, Pure Appl. Geophys., 121, 443–475, 1983.

Rice, J. R., and J.-C. Gu, Earthquake aftereffects and triggered seismic phenomena, Pure Appl. Geophys., 121, 187–219, 1983.

Rice, J. R., and A. L. Ruina, Stability of steady frictional slipping, J. Appl. Mech., 50, 343–349, 1983.

Rice, J. R. and S. T. Tse, Dynamic motion of a single degree of freedom system following a rate and state dependent friction law, J. Geophys. Res., 91, 521–530, 1986.

Ruina, A. L., Friction laws and instabilities: A quasistatic analysis of some dry frictional behavior, Ph.D. thesis, Brown Univ., Providence, R.I., 1980.

Ruina, A. L., Slip instability and state variable friction laws, J. Geophys. Res., 88, 10,359–10,370, 1983.

Ruina, A. L., Constitutive relations for frictional slip, in Mechanics in Geomaterials, edited by Z. P. Bazant, pp. 169–187, John Wiley, New York, 1984.

Scholz, C. H., and J. T. Engelder, The role of asperity indentation and ploughing in rock friction, I, Asperity creep and stick-slip, Int. J. Rock Mech. Min. Sci. Geomech. Abstr., 13, 149–154, 1976.

Shimamoto, T., and J. M. Logan, Velocity-dependent behavior of simulated halite shear zones: An analog for silicates, in Earthquake Source Mechanics, Geophys. Monogr. Ser., vol. 37, edited by S. Das, J. Boatwright, and C. H. Scholz, pp. 44–64, AGU, Washington, D. C., 1986.

Sibson, R. H., Fault rocks and fault mechanisms, J. Geol. Soc. London, 133, 191–213, 1977.

Sibson, R. H., Fault zone models, heat flow, and the depth distribution of earthquakes in the continental crust of the United States, Bull. Seismol. Soc. Am., 72, 151–163, 1982.

Sibson, R. H., Continental fault structure and the shallow earthquake source, J. Geol. Soc. London, 140, 741–767, 1983.

Sibson, R. H., Roughness at the base of the seismogenic zone: Contributing factors, J. Geophys. Res., 89, 5791–5799, 1984.

Solberg, P., and J. D. Byerlee, A note on the rate sensitivity of frictional sliding of Westerly granite, J. Geophys. Res., 89, 4203–4205, 1984.

Stesky, R. M., The mechanical behavior of faulted rock at high temperature and pressure, Ph.D. thesis, Mass. Inst. of Technol., Cambridge, 1975.

Stesky, R. M., Mechanisms of high temperature frictional sliding in Westerly granite, Can J. Earth Sci., 15, 361–375, 1978.

Stuart, W. D., Strain softening prior to two-dimensional strike slip earthquakes, J. Geophys. Res., 84, 1063–1070, 1979a.

Stuart, W. D., Strain softening instability model for the San Fernando earthquake, Science, 203, 907–910, 1979b.

Stuart, W. D., and G. M. Mavko, Earthquake instability on a strike slip fault, J. Geophys. Res., 84, 2153–2160, 1979.

Tse, S. T., Mechanics of crustal strike-slip earthquakes in relation to frictional constitutive response, Ph.D. thesis, Harvard Univ., Cambridge, Mass., 1985.

Tse, S. T., and J. R. Rice, Stick-slip confinement to the upper crust by temperature dependent frictional slip response (abstract), Eos Trans. AGU, 65, 993, 1984.

Tse, S. T., R. Dmowska, and J. R. Rice, Stressing of locked patches along a creeping fault, Bull. Seismol. Soc. Am., 75, 709–736, 1985.

Tullis, T. E., and J. D. Weeks, Constitutive behavior and stability of frictional sliding of granite, Pure Appl. Geophys., in press, 1986.

Vaughan, P., and J. D. Byerlee, Frictional sliding in saturated Westerly granite: Effect of slip rate, paper presented at the 5th Maurice Ewing Symposium, Earthquake Source Mechanics, Lamont-Doherty Geol. Obs. of Columbia Univ., Harriman, N.Y., May 20–23, 1985.

Walsh, J. B., Mechanics of strike-slip faulting with friction, J. Geophys. Res., 73, 761–776, 1968.

Weeks, J., and T. Tullis, Frictional behavior of dolomite (abstract), Eos Trans. AGU, 65, 1077, 1984.

Weeks, J., and T. Tullis, Frictional behavior of dolomite: A variation in constitutive behavior, J. Geophys. Res., 90, 7821–7826, 1985.

Wesson, R. L., R. O. Burford, and W. L. Ellsworth, Relationship between seismicity, fault creep, and crustal loading along the central San Andreas fault, Proceedings, Conference on Tectonic Problems of the San Andreas Fault System, edited by R. L. Kovach and A. Nur, Stanford Univ. Publ. Geol. Sci., 13, 303–321, 1973.

J. R. Rice, Division of Applied Sciences, Harvard University, Pierce Hall, Cambridge, MA 02138.

S. T. Tse, AT&T Bell Laboratories, 600 Mountain Avenue, Murray Hill, NJ 07974.